Zoology 160 (2023) 126108

Contents lists available at ScienceDirect

Zoology

journal homepage: www.elsevier.com/locate/zool

Cranial asymmetry in odontocetes: a facilitator of sonic exploration?

Maíra Laeta [a,*], João A. Oliveira [a], Salvatore Siciliano [b,c], Olivier Lambert [d], Frants H. Jensen [e,f,g], Anders Galatius [e,*]

[a] Setor de Mastozoologia, Departamento de Vertebrados, Museu Nacional/Universidade Federal do Rio de Janeiro, 20941-160 Rio de Janeiro, RJ, Brazil
[b] Departamento de Ciências Biológicas, Escola Nacional de Saúde Pública Sergio Arouca/Fiocruz, 21040-360 Rio de Janeiro, RJ, Brazil
[c] Grupo de Estudos de Mamíferos Marinhos da Região dos Lagos (GEMM-Lagos), Rua São José, 1.260, Praia Seca, 28970-000 Araruama, RJ, Brazil
[d] D.O. Terre et Histoire de la Vie, Institut royal des Sciences naturelles de Belgique, 1000 Brussels, Belgium
[e] Section for Marine Mammal Research, Department of Ecoscience, Aarhus University, Frederiksborgvej 399, 4000 Roskilde, Denmark
[f] Biology Department, Woods Hole Oceanographic Institution, 266 Woods Hole Rd, MA 02543, USA
[g] Biology Department, Syracuse University, 107 College Place, Syracuse, NY 13244, USA

ARTICLE INFO

Keywords:
Odontoceti
Directional asymmetry
Skull morphology
Echolocation source level
Size

ABSTRACT

Directional cranial asymmetry is an intriguing condition that has evolved in all odontocetes which has mostly been associated with sound production for echolocation. In this study, we investigated how cranial asymmetry varies across odontocete species both in terms of quality (*i.e.*, shape), and quantity (magnitude of deviation from symmetry). We investigated 72 species across all ten families of Odontoceti using two-dimensional geometric morphometrics. The average asymmetric shape was largely consistent across odontocetes – the rostral tip, maxillae, antorbital notches and braincase, as well as the suture crest between the frontal and interparietal bones were displaced to the right, whereas the nasal septum and premaxillae showed leftward shifts, in concert with an enlargement of the right premaxilla and maxilla. A clear phylogenetic signal related to asymmetric shape variation was identified across odontocetes using squared-change parsimony. The magnitude of asymmetry was widely variable across Odontoceti, with greatest asymmetry in Kogiidae, Monodontidae and Globicephalinae, followed by Physeteridae, Platanistidae and Lipotidae, while the asymmetry was lowest in Lissodelphininae, Phocoenidae, Iniidae and Pontoporiidae. Ziphiidae presented a wide spectrum of asymmetry. Generalized linear models explaining magnitude of asymmetry found associations with click source level while accounting for cranial size. Using phylogenetic generalized least squares, we reconfirm that source level and centroid size significantly predict the level of cranial asymmetry, with more asymmetric marine taxa generally consisting of bigger species emitting higher output sonar signal, *i.e.* louder sounds. Both characteristics theoretically support foraging at depth, the former by allowing extended diving and the latter being adaptive for prey detection at longer distances. Thus, cranial asymmetry seems to be an evolutionary pathway that allows odontocetes to devote more space for sound-generating structures associated with echolocation and thus increases biosonar search range and foraging efficiency beyond simple phylogenetic scaling predictions.

1. Introduction

Directional asymmetry is the expression of a feature with consistent laterality, ranging from atomic level to bodily features (Neville, 1976; Palmer, 2009). In Cetacea (originating during the early Eocene ~54 Mya) (Thewissen *et al.*, 2001), directional asymmetry has mostly been described in internal structures, including the skeleton (Arvy, 1977). The post-cranial skeleton presents some examples of directionality in asymmetry (Arvy, 1977), such as the appendicular skeleton of some odontocetes (toothed whales) with larger structures on the right side, suggesting lateralized behaviour for swimming, foraging and social interaction (Galatius, 2005, 2006; Gómez-Campos *et al.*, 2010). Most descriptions of cetacean asymmetry, however, relate to cranial structures. The observed asymmetries are unique among mammals and have drawn attention for a long time (Beddard, 1900; Ness, 1967; Mead, 1975). They have been investigated in association with sound production and hearing with diverse interpretations (Cranford *et al.*, 1996; Fahlke and Hampe, 2015; Coombs *et al.*, 2020; Laeta *et al.*, 2020). In some stem Cetacea (archaeocetes) from the late Eocene-Oligocene, skull asymmetry has been proposed to be related to directional hearing

* Corresponding authors.
E-mail addresses: mairalaeta@gmail.com (M. Laeta), agj@ecos.au.dk (A. Galatius).

https://doi.org/10.1016/j.zool.2023.126108
Received 16 May 2023; Received in revised form 31 July 2023; Accepted 4 August 2023
Available online 6 August 2023
0944-2006/© 2023 The Authors. Published by Elsevier GmbH. This is an open access article under the CC BY license (http://creativecommons.org/licenses/by/4.0/).

(Fahlke *et al.*, 2011; Fahlke and Hampe, 2015). The suborder Odontoceti presents a broad spectrum of cranial asymmetry in terms of both shape variation and magnitude. These cranial asymmetries have mostly been associated with sound production (Mead, 1975; Heyning, 1989; but see Macleod *et al.*, (2007) for an alternative interpretation related to prey swallowing).

Cranial asymmetry in many extinct odontocete taxa is less conspicuous, or even absent compared to manifestations in extant taxa (Barnes, 1978 *apud* Ichishima *et al.*, 1994; Barnes, 1985 *apud* Ichishima, 1994; Coombs *et al.*, 2020). The diversity in extinct taxa also includes inconsistencies in directionality, with some structures larger on the right side, as described for *Cotylocara macei* Geisler, Colbert and Carew, 2014 and *Waipatia maerewhenua* (Fordyce, 1994; Fordyce, 1994; Geisler *et al.*, 2014), although in many geologically younger taxa, there is a tendency towards asymmetry with an expression similar to that observed in modern taxa (Marx *et al.*, 2016). This asymmetry may be related to the specialization of the nasal apparatus to sound production for echolocation as suggested for crown odontocetes (Fordyce, 2002; Geisler *et al.*, 2014; Murakami *et al.*, 2014; Boessenecker *et al.*, 2017). In extant species, asymmetry is consistent in directionality as well as with respect to the bone structures involved, but magnitude and shape are variable (Mead, 1975; Heyning, 1989; Laeta *et al.*, 2020). This may reflect adaptations in the soft tissues responsible for sound production and propagation – nasal apparatus and melon, which in turn may be related to sound production (Norris, 1964 and Wood, 1964 *apud* Mead, 1975; Mckenna *et al.*, 2012; Hirose *et al.*, 2015).

In all extant odontocetes, directional asymmetry is characterized by a leftward shift of the right premaxilla and nasal bones, accompanied by left-sided displacement of the dorsal midline in combination with an enlargement of the right nasal bone, premaxilla and maxilla (Mead, 1975; Galatius and Goodall, 2016; Laeta *et al.*, 2020), albeit the amount of asymmetry varies widely. In extant members of the earliest diverging families, the sperm whales (*Physeter* and *Kogia*) and the riverine, *Platanista*, asymmetry is remarkable, while most of the beaked whales (Ziphiidae) and other 'river dolphins' *Inia* and *Pontoporia* present more subtle asymmetry (Ness, 1967; Hirose *et al.*, 2015; Huggenberger *et al.*, 2016a). Extant members of the latest diverging families, Monodontidae, Phocoenidae and Delphinidae, forming the superfamily Delphinoidea (Milinkovitch *et al.*, 1994; Waddell *et al.*, 2000; McGowen *et al.*, 2020), present highly variable levels of asymmetry (Ness, 1967; Galatius and Goodall, 2016; Laeta *et al.*, 2020).

Cranford *et al.* (1996) hypothesized a relationship between level of asymmetry and sound production, suggesting that less asymmetric odontocetes, *e.g. Pontoporia* and Phocoenidae, emitted clicks with a single peak in frequency because they were generated simultaneously and bilaterally from similarly sized phonic lips. More asymmetric taxa, *e.g.* the bottlenose dolphin *Tursiops truncatus* (Montagu, 1821), were then hypothesized to emit clicks with two spectral peaks as a consequence of the asymmetric dimensions of right and left phonic lips. Subsequently, Madsen *et al.* (2010, 2013) and Ames *et al.* (2020) investigated several representatives of Delphinoidea, and detected click production only from the right pair of phonic lips in the subtly asymmetric harbour porpoise *Phocoena phocoena* (Linnaeus, 1758), as well as in more asymmetric species, such as *T. truncatus*, false killer whale *Pseudorca crassidens* (Owen, 1846), and beluga whale *Delphinapterus leucas* (Pallas, 1776).

Further studies investigating the relationship between magnitude of asymmetry and frequencies of echolocation clicks among odontocete taxa have not detected a clear signal. Huggenberger *et al.* (2016a) compared the highly asymmetric *Kogia sima* (Owen, 1866) and the subtly asymmetric *Pontoporia blainvillei* (Gervais and d'Orbigny, 1844), the phocoenids *P. phocoena* and *Phocoenoides dalli* (True, 1885), and the delphinid *Cephalorhynchus commersonii* (Lacépède, 1804), all of which emit clicks with a single peak frequency (also known as narrow-band high frequency clicks). Within the Lissodelphininae, which include species with varying levels of asymmetry emitting clicks with both single and dual spectral peaks in frequency, there is no association between magnitude of asymmetry and type of echolocation signal (Galatius and Goodall, 2016; Jensen *et al.*, 2018; Galatius *et al.*, 2019). Thus, this aspect of echolocation signals does not appear to be related to the level of cranial asymmetry. Coombs *et al.* (2020) detected a potential signal of echolocation frequency contributing to evolution of odontocete cranial asymmetry and called for further analysis of species-specific frequencies across Cetacea. Laeta *et al.* (2020) investigated relationships of source level, frequency, duration and bandwidth among Delphinoidea, and found that, among these characteristics, source level provided the strongest signal. The interpretation was that asymmetry was associated with the enlargement of the sound-generating structures on the right side, allowing the production of more powerful sounds, ultimately enabling the scanning of larger volumes of water, particularly by deep-diving members of the superfamily.

Here, we analyze the variation of directional cranial asymmetry across all ten families of the suborder Odontoceti. We investigate the nature of asymmetry in terms of shape as well as the magnitude of asymmetry through two-dimensional geometric morphometrics. We also investigate potential relationships between these expressions of asymmetry and aspects of sound production – source level and frequency, with further implications for adaptations to diverse habitats, such as rivers, coastal systems or deep oceanic waters.

2. Material and methods

2.1. Sample

The investigated sample comprises 346 skulls of 72 species and one hybrid, encompassing all ten families of Odontoceti, which are held in the Museu Nacional - Universidade Federal do Rio de Janeiro, Brazil (MN); Grupo de Estudos de Mamíferos Marinhos do Rio Grande do Sul, Brazil (GEMARS); Museo Nacional de Historia Natural, Chile (MNHN-Chile); Natural History Museum of Denmark, Denmark (NHMDK); Natural History Museum, London, United Kingdom (NHMUK); Muséum national d'Histoire naturelle, France (MNHN-France); Museo di Storia Naturale dell'Università di Pisa, Italy (MSNUP); Museum of New Zealand Te Papa Tongarewa, New Zealand (Te Papa); California Academy of Sciences, United States of America (CAS:MAM); Florida Museum of Natural History, United States of America (UF-Mammals); National Museum of Natural History, Smithsonian Institution, United States of America (USNM); Natural History Museum of Los Angeles County, United States of America (LACM); San Diego Natural History Museum, United States of America (SDNHM); The Charleston Museum, United States of America (ChM); and University of Alaska Museum, United States of America (UAM:Mamm). Data from part of the skulls analyzed from NHMUK and USNM, and of all skulls from LACM and SDNHM were obtained from Goswami (2015); Sabin *et al.* (2018). Information on specimens is compiled in Supporting Information, Tables S1 and S2.

Skulls were selected considering their completeness to allow the correct identification of taxa and inclusion of anatomical structures where the morphometric landmarks were plotted, aiming to obtain a high taxonomic diversity encompassing the ten currently recognized families of odontocetes. The identification of cranial structures was based on Mead and Fordyce (2009), Velez-Juarbe *et al.*, (2015) and Huggenberger *et al.*, (2016b). The skull sample was not separated by sex or age estimation, given the current absence of this information for most specimens. Most specimens were sub-adult or adult as assessed through fusion of the skull bones. The small set of physically immature individuals showing incomplete fusion of cranial sutures is listed in Supporting Information (Supporting Information, Table S1).

2.2. Skull image acquisition

To investigate cranial asymmetry, we used bidimensional images of the dorsal aspect of the skulls obtained from two types of data: (1)

standardized photographs to avoid errors caused by equipment, parallax, or reliability of landmarks, and (2) skull surface and CT scans.

For the photographed skulls, a portable tripod or copy stand were used, most being equipped with a bubble level. A Nikon™ D610 equipped with a Nikon™ AF-S DX Nikkor 24–85 mm f/3.5–4.5 ED VR lens, a Nikon™ D7000 equipped with a Nikon™ AF-S DX Nikkor 18–105 mm f/3.5–5.6 ED VR lens, a Canon™ EOS 1000D equipped with a Canon™ 25–40 mm f/4.5 lens and a Canon™ 5D equipped with a Contax Carl Zeiss Makro-Planar™ 60 mm f/2.8 lens were used to photograph skulls in dorsal view. Most skulls were placed on a mat (A1 format, 620 × 900 × 2 mm) and centered using the greatest length and width of the skull. To ensure that the camera and the mat were in parallel planes, a second bubble level was placed on the mat. The focal distance was adjusted by zooming the lens to cover the sensor area with the skull as much as possible. A scale square of 1 × 1 cm placed in a similar location was used as a reference. The skull sagittal plane was delimited as a straight line between the midpoint of the rostral tip and the dorsal margin of the *foramen magnum* to bilaterally divide this structure. This posteriormost dorsal point was highlighted with a pencil since the *foramen magnum* landmark location was not visible in all skulls after positioning them on the mat. For almost all taxa, the camera was located at a distance of 90 cm to the mat, except for Ziphiidae, which were photographed at a distance of 220 cm. Another exception was *Cephalorhynchus hectori* (Te Papa MM002607) being photographed on a homogeneous dark background about 200–250 cm from the camera parallel to the base without using a bubble level, with the centimeter grid positioned diagonally from the usual position.

To validate measurement errors in the repeatability and reliability of plotting anatomical landmarks, a sample of 150 specimens, containing representatives from all ten families of odontocetes, were photographed twice.

The image files (*.jpeg) were imported to a computer using Adobe™ Lightroom (version 4.4) to correct the inherent lens distortions by implementing a specific profile adjustment for each lens.

Images of scanned skulls were obtained from file extensions *.DICOM using the software InVesalius™ (version 3.1.1) (Amorim *et al.*, 2015). Then, to generate digitized images with *.gltf, *.obj, *.ply and *.stl extensions, the skull was positioned in the frontal plane, parallel to the dorsal view, with a scaled grid respecting its greatest length and width using the software Blender™ (version 2.92) (Community B.O., 2018). In this scanned sample, the sagittal plane was also delimited as a straight line between the midpoint of the rostral tip and the dorsal margin of the *foramen magnum*, after highlighting the most posterior dorsal point of the latter, which is not visible in dorsal view in all skulls when positioned for photography in the dorsal aspect. A square of 1 × 1 cm located in a comparable position among the photographed specimens was used as a reference for scale.

2.3. Landmark data acquisition

Shape variation was investigated using 31 homologous anatomical landmarks (LMs) applying two-dimensional geometric morphometrics to characterize the shape profile and the spectrum of magnitude of directional asymmetry (Bookstein, 1991), in addition to testing the measurement error in all families of odontocetes. Landmark selection followed geometric morphometric studies of odontocete crania (Fig. 1; Table 1) (Monteiro-Filho *et al.*, 2002; Galatius and Goodall, 2016; Laeta *et al.*, 2020). Absence of nasal bone(s) in *Physeter* and Kogiidae restricted the inclusion of anatomical landmarks around this structure. To include variation close to the nasal bones, we added an anatomical landmark at the suture between the right and left frontal bones. The studied set of landmarks included points along the sagittal plane and bilateral paired landmarks on each side of the skull.

Table 1
Description of the anatomical landmarks used in this study, depicted in Fig. 1.

Landmark	Landmark description
1	Midpoint of the rostral tip
2	Dorsal margin of the *foramen magnum*
3	Anterior-most point of left maxilla
4	Anterior-most point of right maxilla
5	Anterior-most point in the left frontomaxillar border
6	Anterior-most point in the right frontomaxillar border
7	Left antorbital notch
8	Right antorbital notch
9	Lateral-most extension of left frontomaxillar border
10	Lateral-most extension of right frontomaxillar border
11	Posterior-most expansion of left frontoparietal suture
12	Posterior-most expansion of right frontoparietal suture
13	Posterior-most point on the curve of the left parietal bone
14	Posterior-most point on the curve of the right parietal bone
15	Posterior-most point on the curve of the left occipital condyle
16	Posterior-most point on the curve of the right occipital condyle
17	Posterior margin of anterior-most left infraorbital foramen
18	Posterior margin of anterior-most right infraorbital foramen
19	Maximum deflection point of left nasal opening
20	Maximum deflection point of right nasal opening
21	Lateral-most extension of left premaxilla in the posterior portion
22	Lateral-most extension of right premaxilla in the posterior portion
23	Posterior-most extension of left premaxilla
24	Posterior-most extension of right premaxilla
25	Maximum deflection point of left maxilla
26	Maximum deflection point of right maxilla
27	Posterior-most extension of left maxilla
28	Posterior-most extension of right maxilla
29	Midpoint of bony nasal septum at anterior border of bony nares
30	Anterior-most point of the suture between the frontal bones
31	Anterior-most point of the suture crest between the frontal and interparietal bones (Galatius and Goodall, 2016)

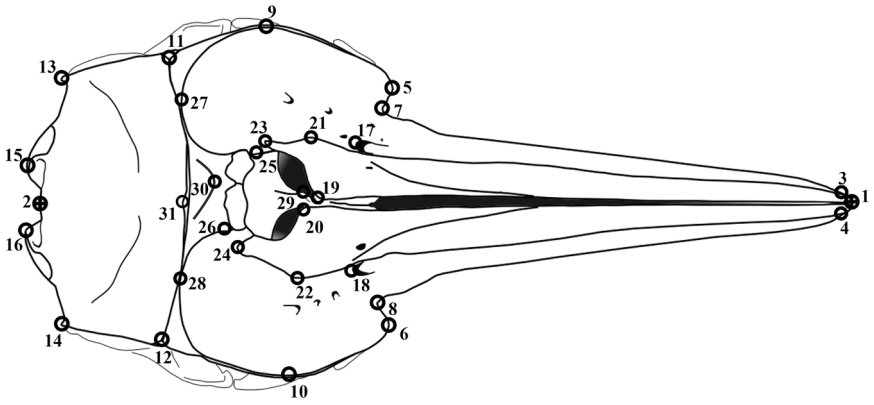

Fig. 1. Two-dimensional landmarks shown in skull dorsal aspect of a representative odontocete, the Guiana dolphin *Sotalia guianensis*. Landmark descriptions are given in Table 1.

Our database of digital skull images in dorsal view was compiled using the TPSUtil™ (version 1.76) software (Rohlf, 2015). Bidimensional Cartesian sets of landmark coordinates (x and y) were accessed by manipulating images – stored in *.tps format, in the TPSDig™ (version 2.31) software (Rohlf, 2015).

Despite our effort to select complete specimens, some landmarks could not be identified on the photographs, or the structures were missing from key taxa. In these cases, landmark positions were estimated with the software R (version 4.2.2) (R Core Team, 2022) using the 'estimate.missing' function with the thin plate spline option of the 'geomorph' R package (version 3.2.0) (Adams *et al.*, 2020). Usually, the specimens concerned were compared with their conspecifics, however *Mesoplodon densirostris, Mesoplodon layardii*, *Mesoplodon carlhubbsi*, *Mesoplodon perrini*, *Mesoplodon peruvianus*, *Sousa teuszii* and *Orcaella heinsohni* were compared with their congeners, and *Hyperoodon ampullatus* was compared with the other representatives of the family Ziphiidae for the estimation of missing landmarks (Supporting Information, Table S1).

To measure the accuracy of landmark digitalization (Arnqvist and Mårtensson, 1998; Klingenberg and McIntyre, 1998), we quantified the error between repeated landmarking images for 150 representatives of all families using Dahlberg's error, $\sqrt{\sum d^2/2N}$, where "d" is the difference between the landmarks from the first and second digitalization and "N" represents the sample size (Kim, 2013).

2.4. Shape analyses

Statistical analyses of shape variation regarding cranial asymmetry were performed using the software MorphoJ™ (version 1.06d) (Klingenberg, 2011). Bi-dimensional landmark coordinates computed with TPSDig™ were imported to MorphoJ™, under the 'object symmetry' configuration. Generalized Procrustes Analysis (GPA) allowed us to acquire skull shape information after removing translation, scaling, and rotation effects from each landmark configuration through superimposition of the centroids (Rohlf and Slice, 1990; Dryden and Mardia, 1998; Klingenberg *et al.*, 2002). Subsequently to GPA, the resulting landmark configuration of each specimen was compared to the standard symmetrical average shape, and the residuals provided the asymmetric shape configuration (Klingenberg *et al.*, 2002). This individual asymmetric component was used to identify and analyse the quality (*i.e.*, shape) and quantity (*i.e.*, magnitude) of directional asymmetry, as well as in the downstream statistical analyses.

To map the relationship of shape variation from residuals of the symmetrical average shape among taxa, as well as its distribution along main trends of variation, Principal Component Analysis (PCA) was performed using the asymmetric component of shape in MorphoJ™ software.

Centroid size (CS), a metric for skull size independent of shape was calculated for each specimen by the square root of the sum of squared distances of all landmarks to the averaged coordinates of the landmark configuration (Zelditch *et al.*, 2012). CS was used to perform exploratory analyses in order to evaluate the magnitude of asymmetry in relation to taxa size and echolocation click characteristics.

2.5. Quality of directional asymmetry

The presence of a phylogenetic signal in the asymmetrical component of shape was tested in a subset including most species, based on the molecular phylogeny of McGowen *et al.* (2020). The monodontid hybrid and the species *Phocoena sinus*, *Sousa plumbea*, *Sousa sahulensis*, *Sousa teuszii*, *Sotalia fluviatilis*, *Lagenorhynchus cruciger*, *Cephalorhynchus eutropia*, *C. hectori* and *Tursiops truncatus gephyreus*, were excluded from this analysis as they are not represented in the phylogenetic tree. To identify the presence of a phylogenetic signal, a permutation test was used applying 'weighted' and 'unweighted' squared-change parsimony calculation on the rooted tree by 10,000 randomizations with the software MorphoJ™ (version 1.06d) (Klingenberg and Gidaszewski, 2010; Klingenberg, 2011).

To characterize asymmetrical shape for each species, we calculated the mean directionality of the average asymmetry from the average symmetric shape. These mean directionalities of vectors were then compared between all species pairs, implementing the function 'VecCompare6' of the software IMP™, with 900 bootstrap sets (Sheets, 2007).

2.6. Quantification of directional asymmetry

The magnitude of asymmetry for each specimen was defined as the partial Procrustes distance of the asymmetric component of shape to the corresponding symmetric component. Species and taxon means were derived from these values.

2.7. Asymmetry's relation to sound production

The relationships between species-specific sound production characteristics, habitat use and skull size on the one hand and cranial asymmetry on the other hand were investigated using the compiled information on species-specific parameters of sound production: peak-to-peak source level (SL) and centroid frequency (cF). Furthermore, information on diving behaviour was represented by the maximum known dive depth (Depth) and size was represented by the median of CS (Table 2). Only the parameters SL, cF and CS were used as independent variables to model the species-specific median of magnitude of cranial asymmetry in Generalized Linear Models (GLMs).

The data were analysed twice with different species composition as the sound production parameters for *Kogia sima* (Malinka *et al.*, 2021) and *Globicephala macrorhynchus* (Pedersen *et al.*, 2021) were estimated with some caveats. The authors considered that the source levels estimated in these studies may not be representative of the maximum capacity of these species during deep water foraging. Thus, we analyzed a main dataset including the maximum estimated values of all parameters of sound production for all species, as well as a supplementary dataset excluding *K. sima* and *G. macrorhynchus*.

Parameters of sound production and body size are related, with large animals generally producing louder sounds with lower centroid frequency (Jensen *et al.*, 2018). Thus, we investigated the correlation of each sound parameter – SL and cF, with median centroid size using the function 'cor.test' with the 'Spearman' option in R through 'stats' package (version 4.2.2) (R Core Team, 2022). For variables with significant and strong correlation, linear regression models on the natural logarithm (to obtain a linear relationship) of these sound parameters on CS were performed using the function 'lm' in R 'stats' package (version 4.2.2) (R Core Team, 2022). Residuals from these models were then used to represent the concerned sound variables in downstream analyses. Exploratory GLMs including all combinations of the sound variables SL and cF, as well as centroid size, were conducted including the species for which information for all variables were available, using the 'glm' function with Gamma error distribution and inverse link function in R implementing the 'stats' package (version 4.2.2) (R Core Team, 2022). To identify the best performing models for both datasets, we performed analyses of second-order Akaike Information Criterion (AICc) using delta < 2 (Burnham and Anderson, 2002; Burnham *et al.*, 2011; Table 2), by applying the functions 'model.sel' and 'dredge' using 'MuMIn' package (version 1.43.17) (Bartón, 2020) in R. After the AICc selection, final GLMs were performed including species presenting all the predictor variables contained in the selected models.

Then, the AICc-selected models were repeated using Phylogenetic Generalized Least Squares (PGLS) based on the molecular phylogeny of McGowen *et al.* (2020), to investigate the potential effects of phylogeny on the relation between the magnitude of asymmetry and explanatory variables (Pagel, 1999; Table 2). PGLS analysis was performed in R using

Table 2
Estimated values of median of species-specific magnitude of asymmetry, median of centroid size (CS), maximum dive depth – Depth (in meters), peak to peak source level – SL (dB re 1μPa at 1 m) and centroid frequency – cF (kHz) for specimens of the suborder Odontoceti used in the Generalized Linear Models (GLMs) with analyses of second-order Akaike Information Criterion (AICc), and Phylogenetic Generalized Least Squares (PGLS). ✳ maximum bottom depth estimated in the literature according to the environment bathymetry; ◆ depth estimated in the literature according to prey distribution; • received source level; ■ maximum values of sound parameters.

Families / Subfamilies	Species	Magnitude of asymmetry	Centroid size – CS	Depth (m)	Source level – SL (dB)	Centroid frequency – cF (kHz)	References
Physeteridae	*Physeter macrocephalus* (Pm)	0.0597	467.06	≥ 2250	240	15	Whitney (1968) *apud* Tyack *et al.*, 2006; Norris and Harvey (1972) *apud* Best, 1999; Madsen *et al.*, 2002; Møhl *et al.*, 2003; Zimmer *et al.*, 2005a; Jensen *et al.*, 2018
Kogiidae	*Kogia sima* (Ks)	0.0972	50.64	≈ 1300◆	197■	129■	Maigret and Robineau (1981) *apud* Plön, 2004; Malinka *et al.*, 2021
Kogiidae	*Kogia breviceps* (Kb)	0.1008	82.37	≈ 1400◆	-	129	Nesis (1987) *apud* Plön, 2004; Madsen *et al.*, 2005
Platanistidae	*Platanista gangetica* (Pg)	0.0536	56.19	≥ 120✳	183	61	Miller *et al.*, 2009; Jensen *et al.*, 2013
Ziphiidae	*Berardius bairdii* (Bb)	0.0267	164.14	1777	-	28	Minamikawa *et al.*, 2007; Stimpert *et al.*, 2014
Ziphiidae	*Berardius arnuxii* (Ba)	0.0303	146.00	-	-	-	-
Ziphiidae	*Tasmacetus shepherdi* (Ts)	0.0236	183.69	≥ 1500✳	-	-	Donnelly *et al.*, 2018
Ziphiidae	*Ziphius cavirostris* (Zc)	0.0485	130.89	2992	214	42	Zimmer *et al.*, 2005b; Schorr *et al.*, 2014
Ziphiidae	*Hyperoodon planifrons* (Hp)	0.0477	169.79	-	-	-	-
Ziphiidae	*Hyperoodon ampullatus* (Ha)	0.0549	191.97	2339	203	43	Wahlberg *et al.*, 2011a; Miller *et al.*, 2015
Ziphiidae	*Mesoplodon bidens* (Mb)	0.0295	153.79	≈ 1500✳	-	38	Cholewiak *et al.*, 2013; NOAA, 2022a
Ziphiidae	*Mesoplodon ginkgodens* (Mk)	0.0424	110.76	-	-	-	-
Ziphiidae	*Mesoplodon mirus* (Mi)	0.0208	116.44	-	-	-	-
Ziphiidae	*Mesoplodon europaeus* (Me)	0.0201	114.45	-	-	38	Jensen *et al.*, 2018
Ziphiidae	*Mesoplodon layardii* (My)	0.0599	127.88	-	-	-	-
Ziphiidae	*Mesoplodon carlshubbsi* (Mc)	0.0230	98.90	-	-	-	-
Ziphiidae	*Mesoplodon bowdoini* (Mw)	0.0495	118.67	-	-	-	-
Ziphiidae	*Mesoplodon hectori* (Mh)	0.0400	107.68	-	-	-	-
Ziphiidae	*Mesoplodon grayi* (Mg)	0.0451	123.64	-	-	-	-
Ziphiidae	*Mesoplodon stejnegeri* (Ms)	0.0298	108.31	≥ 1500✳	-	-	NOAA, 2022b
Ziphiidae	*Mesoplodon densirostris* (Md)	0.0353	117.80	1888	211	33	Joyce *et al.*, 2017; Jensen *et al.*, 2018
Ziphiidae	*Mesoplodon perrini* (Mr)	0.0446	150.60	≥ 1000✳	-	-	Dalebout *et al.*, 2002
Ziphiidae	*Mesoplodon peruvianus* (Mu)	0.0388	129.26	-	-	-	-
Lipotidae	*Lipotes vexillifer* (Lv)	0.0509	82.74	-	-	-	-
Iniidae	*Inia geoffrensis* (Ig)	0.0286	75.95	≥ 100✳	190	101	Sioli, 1984; Ladegaard *et al.*, 2015
Pontoporiidae	*Pontoporia blainvillei* (Pb)	0.0129	59.41	≈ 50✳	-	-	Crespo, 2009; Danilewicz *et al.*, 2009; Melcón *et al.*, 2012; Amaral *et al.*, 2018
Monodontidae	Hybrid *Delphinapterus leucas* (Dl) x *Monodon monoceros* (Mm)	0.0863	123.71	-	-	-	-
Monodontidae	*Delphinapterus leucas* (Dl)	0.0739	82.66	1275	218	-	Au *et al.*, 1987; Richard *et al.*, 1998
Monodontidae	*Monodon monoceros* (Mm)	0.0877	96.19	≥ 1400	210	53	Laidre *et al.*, 2003; Rasmussen *et al.*, 2015; Jensen *et al.*, 2018
Phocoenidae	*Neophocaena phocaenoides* (Np)	0.0259	34.31	< 50✳	-	-	Jefferson and Moore, 2020
Phocoenidae	*Neophocaena asiaeorientalis* (Na)	0.0242	35.14	< 200✳	178	129	Jefferson *et al.*, 2015; Jensen *et al.*, 2018
Phocoenidae	*Phocoenoides dalli* (Pd)	0.0220	52.18	94	183	137	Hanson and Baird, 1998; Kyhn *et al.*, 2013
Phocoenidae	*Phocoena phocoena* (Pp)	0.0276	41.89	410	186	137	Nielsen *et al.*, 2018; Jensen *et al.*, 2018
Phocoenidae	*Phocoena dioptrica* (Pt)	0.0270	46.55	-	-	-	-
Phocoenidae	*Phocoena spinipinnis* (Pi)	0.0370	36.92	≤ 60✳	-	146	Reyes, 2009; Reyes *et al.*, 2018
Phocoenidae	*Phocoena sinus* (Pu)	0.0346	37.48	≤ 40✳	-	-	Silber, 1990
Delphinidae	*Lagenorhynchus acutus* (Lc)	0.0338	66.62	≈ 100✳	-	-	Winn, 1982
Delphinidae	*Lagenorhynchus albirostris* (La)	0.0544	76.10	< 200✳	204	94	Galatius and Kinze, 2016; Jensen *et al.*, 2018
Delphinidae	*Sousa plumbea* (Sp)	0.0308	80.20	< 30✳	-	-	Kiani and Van Waerebeek, 2015
Delphinidae	*Sousa sahulensis* (Ss)	0.0295	84.95	≈ 18	199	106	Parra, 2006; de Freitas *et al.*, 2015
Delphinidae	*Sousa teuzii* (Sz)	0.0195	83.38	-	-	-	-
Delphinidae	*Sotalia fluviatilis* (Sv)	0.0376	49.18	≥ 100✳	181	99	Sioli, 1984; Yamamoto *et al.*, 2015
Orcininae	*Orcinus orca* (Oo)	0.0427	151.46	≈ 767.5	203	37	Eskesen *et al.*, 2011; Reisinger *et al.*, 2015; Jensen *et al.*, 2018
Lissodelphininae	*Lissodelphis borealis* (Lb)	0.0424	65.33	≈ 250◆	-	-	Fitch and Brownell, 1968
Lissodelphininae	*Lissodelphis peronii* (Lp)	0.0455	64.81	≈ 300◆	-	-	Baker, 1981

(*continued on next page*)

Table 2 (*continued*)

Families / Subfamilies	Species	Magnitude of asymmetry	Centroid size – CS	Depth (m)	Source level – SL (dB)	Centroid frequency – cF (kHz)	References
Lissodelphininae	*Lagenorhynchus obscurus* (Lo)	0.0339	58.32	156	191	81	Bernasconi *et al.*, 2011; Jensen *et al.*, 2018
Lissodelphininae	*Lagenorhynchus obliquidens* (Lq)	0.0330	58.20	≈ 200◆	-	-	Black, 1994
Lissodelphininae	*Lagenorhynchus australis* (Lu)	0.0406	55.86	≈ 20✳	185	129	Heinrich *et al.* (2008) *apud* Goodall, 2009; Kyhn *et al.*, 2010
Lissodelphininae	*Lagenorhynchus cruciger* (Lg)	0.0546	58.78	≈ 200✳	197	128	Jefferson *et al.*, 1993; Kyhn *et al.*, 2009
Lissodelphininae	*Cephalorhynchus commersonii* (Cc)	0.0359	47.23	< 100✳	177	133	Iñíguez and Tossenberger, 2007; Kyhn *et al.*, 2010; Dawson, 2018
Lissodelphininae	*Cephalorhynchus eutropia* (Ce)	0.0354	55.86	≈ 20✳	> 165●	126	Jefferson *et al.*, 2008; Götz *et al.*, 2010
Lissodelphininae	*Cephalorhynchus heavisidii* (Cv)	0.0373	43.65	≤ 200✳	173	125	Morisaka *et al.*, 2011; Gopal *et al.*, 2016
Lissodelphininae	*Cephalorhynchus hectori* (Ct)	0.0388	44.36	< 100✳	177	128	Kyhn *et al.*, 2009; Bräger and Bräger 2018
Globicephalinae	*Orcaella heinsohni* (Oh)	0.0619	49.14	≈ 130✳	200	98	van Andel and Veevers (1967) *apud* Lavering, 1993; de Freitas *et al.*, 2018
Globicephalinae	*Orcaella brevirostris* (Ob)	0.0443	51.21	≈ 110✳	195	95	Anderson (1879) *apud* Stacey and Arnold, 1999; Jensen *et al.*, 2013
Globicephalinae	*Steno bredanensis* (Sb)	0.0431	89.46	399.5	-	-	Shaff and Baird, 2021
Globicephalinae	*Grampus griseus* (Gg)	0.0653	87.78	623	220	75	Madsen *et al.*, 2004; Visser *et al.*, 2021
Globicephalinae	*Pseudorca crassidens* (Pc)	0.0714	101.86	927.5	220	49	Madsen *et al.*, 2004; Baird *et al.*, 2014
Globicephalinae	*Feresa attenuata* (Fa)	0.0646	58.13	364	210	77.5	Jensen *et al.*, 2018; Pulis *et al.*, 2018
Globicephalinae	*Peponocephala electra* (Pe)	0.0561	70.57	471.5	-	-	Joyce *et al.*, 2017; West *et al.*, 2018
Globicephalinae	*Globicephala macrorhynchus* (Gy)	0.0723	118.47	1.019	210■	53■	Aguilar Soto *et al.*, 2008; Pedersen *et al.*, 2021
Globicephalinae	*Globicephala melas* (Ge)	0.0691	114.40	828	196	55	Heide-Jørgensen *et al.*, 2002; Eskesen *et al.*, 2011
Delphininae	*Sotalia guianensis* (Sg)	0.0335	60.90	≤ 35✳	-	-	Azevedo *et al.*, 2007
Delphininae	*Sousa chinensis* (Sh)	0.0355	80.83	≈ 30✳	188	95	Fang *et al.*, 2015; Parra and Jefferson, 2018
Delphininae	*Tursiops truncatus* (Tt)	0.0413	85.69	1000	200	77	Jensen *et al.*, 2018; Fahlman *et al.*, 2023
Delphininae	*Tursiops t. gephyreus* (Tg)	0.0383	90.57	-	-	-	-
Delphininae	*Tursiops aduncus* (Ta)	0.0404	71.21	≈ 200✳	205	99	Wang and Yang, 2009; Wahlberg *et al.*, 2011b; Jensen *et al.*, 2018
Delphininae	*Stenella frontalis* (Sf)	0.0442	63.19	≈ 60	209	86	Davis *et al.*, 1996; Jensen *et al.*, 2015
Delphininae	*Stenella attenuata* (Sa)	0.0426	61.06	213	212	83	Baird *et al.*, 2001; Schotten *et al.*, 2004
Delphininae	*Stenella coeruleoalba* (So)	0.0575	71.92	705	-	-	Minamikawa *et al.*, 2003
Delphininae	*Stenella clymene* (Sc)	0.0450	58.13	≤ 700	-	-	Mullin *et al.*, 1994
Delphininae	*Stenella longirostris* (Sl)	0.0365	57.84	≤ 600◆	208	80	Perrin and Gilpatrick (1994) *apud* Perrin, 2009 ; Dolar *et al.*, 2003; Schotten *et al.*, 2004; Jefferson *et al.*, 2015
Delphininae	*Delphinus delphis* (Dd)	0.0444	65.24	280	-	-	Leatherwood *et al.*, 1982
Delphininae	*Lagenodelphis hosei* (Lh)	0.0534	70.20	≈ 600◆	-	-	Dolar *et al.*, 2003

* In our study, the genus Neophocaena was represented by Neophocaena asiaeorientalis in terms of sound variables while in the phylogenetic tree of McGowen *et al.* 2020, genetics from Neophocaena phocaenoides was representing the genus. Our shape variables for the genus derived only from Neophocaena asiaeorientalis for squared-change parsimony and phylogenetic generalized least squares (PGLS) models, while shape variables from both species were included in other analyses.

'ape' (version 5.4) and 'nlme' packages (version 3.1–153) and applying the function 'gls' with restricted maximum likelihood to fit Pagel's λ correlation, using 'corPagel', and estimate the scaling factor 'λ' under the assumption of Brownian motion (Paradis *et al.*, 2020; Pinheiro *et al.*, 2021).

3. Results

3.1. Shape variation

The Dahlberg's error including representatives from all ten families of odontocetes was 0.003, which represents a lower value than the smallest species-specific deviation from symmetry at a partial Procrustes distance of 0.013, obtained for a specimen of *Pontoporia blainvillei*.

Across all ten odontocete families, skull asymmetries showed similar landmark displacements, demonstrating a relatively consistent pattern, with some taxon-specific differences (Fig. 2A-J). The skull outline in dorsal position, as defined by the rostral tip of the premaxillae, the maxillae, antorbital notches and braincase, as well as the suture crest between frontal and interparietal bones, showed consistent right shifts, while the nasal septum and premaxillae displaced to the left side. Premaxillary and maxillary landmarks presented the greatest variety in displacement, but consistently, the right structure had the greatest dimensions in all species.

Skull shape deviation among the superfamily Physeteroidea showed pronounced posterior extension of the right premaxilla and concomitant shortening of the left structure, in addition to a slight right shift of the suture between frontal bones. This was most pronounced in Kogiidae, which also showed the greatest shape variation, with a remarkable displacement of the nasal septum and anterior dorsal infraorbital foramina to the left. The posteriormost extension of the maxillae displayed a right shift, along with the frontomaxillar borders, with the right structure shifting anteriorly, whereas the left structure moved posteriorly (Fig. 2B). *Physeter macrocephalus* showed a similar displacement of the lateral extension of the frontomaxillar border and presented a marked right shift of the suture crest between the frontal and interparietal. The right maxilla had a remarkable posterior and lateral extension in this species, while the left structure displaced anteriorly (Fig. 2A).

Among the 'river dolphins', the greatest displacement of landmarks was found for *Platanista gangetica*, followed by *Lipotes vexillifer* (Fig. 2C; 2E-G). In *P. gangetica*, the anteriormost and lateral frontomaxillar border of the right maxilla was displaced anteriorly, while the left structure was

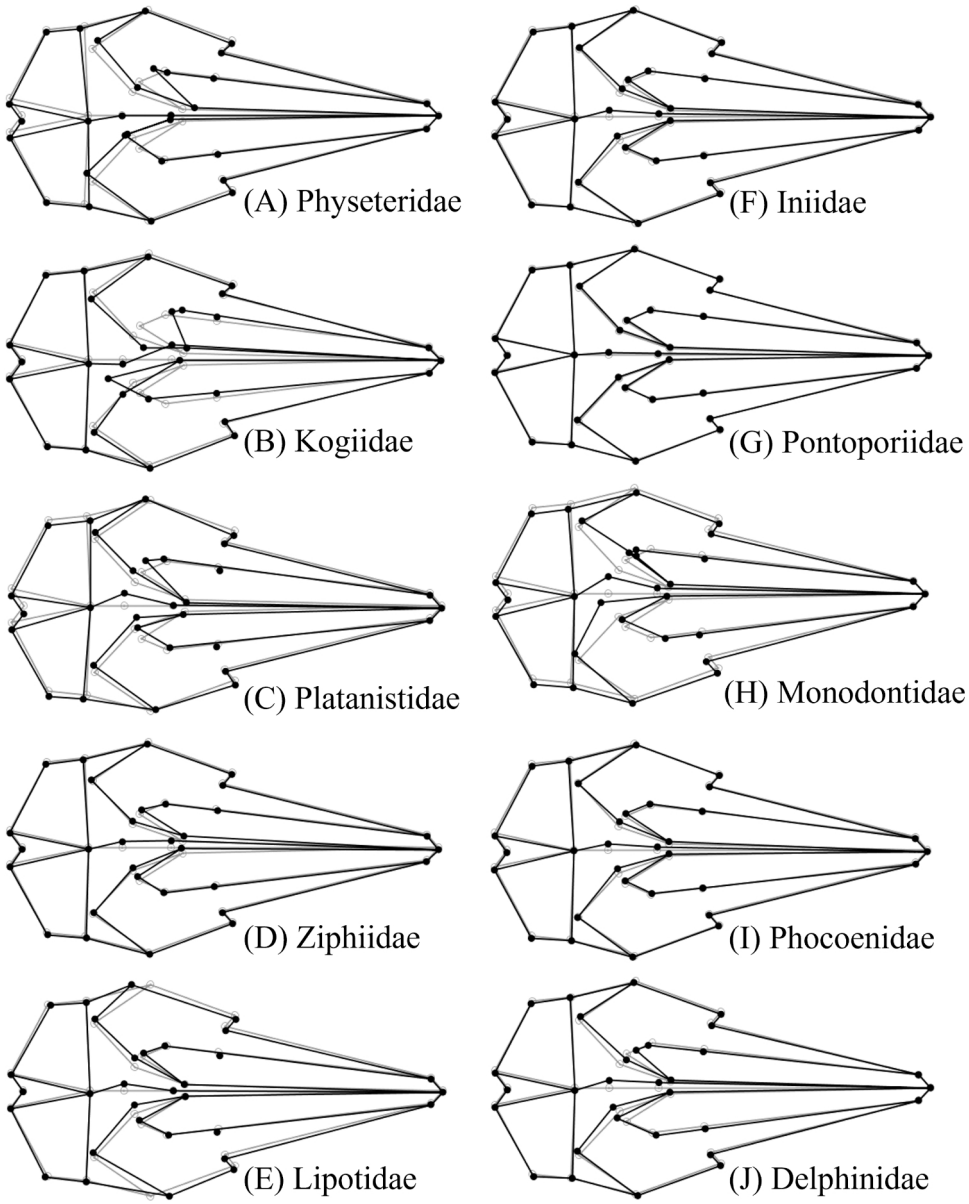

Fig. 2. Average asymmetrical skull shape of the ten families of Odontoceti, in dorsal view, showing asymmetric components (black), overlapping with symmetric components (grey).

displaced posteriorly. The suture between the frontals shifted markedly to the left side, along with the displacement of the premaxillae and maxillae, with the right structures being wider. The braincase shifted noticeably to the right (Fig. 2C). *L. vexillifer* showed greater anterior narrowing and posterior widening at the right frontomaxillar border, while the structures on the left showed an opposite pattern (Fig. 2E). *Inia geoffrensis* and *P. blainvillei* showed slight displacements with an emphasis on the frontomaxillar borders, which presented similar antero-posterior movements between *P. gangetica* and *P. blainvillei*, and between *L. vexillifer* and *I. geoffrensis* (Fig. 2C; 2E-G). In *P. blainvillei*, the landmark displacements were consistent with the general pattern of other odontocetes, showing similarity in directional asymmetry in the bone structures involved (Fig. 2).

Ziphiidae presented posterior extension and widening in the right premaxilla, with the narrower left structure displaced anteriorly (Fig. 2D). The posterior maxillary extension demonstrated a similar pattern to that observed in Kogiidae, with the right maxilla showing a slight shortening and lateral widening relative to the left structure (Fig. 2D).

Among Delphinoidea, the family Monodontidae presented the greatest landmark shifts in the frontomaxillar borders, the widened right border being shifted posteriorly, whereas the narrowed left structure displaced anteriorly, and the braincase presented a substantial right displacement similar to that seen in *P. macrocephalus* and *P. gangetica*. The suture between the frontals showed a marked shift to the left, with the premaxillae also showing a leftward displacement. Furthermore, the right premaxilla was slightly elongated, whereas the left premaxilla was shortened. The right maxilla showed the greatest lateral enlargement, in addition to a posterior extension, whilst the left structure is consistently narrower (Fig. 2H). Delphinidae presented an anterior displacement of the lateralmost extension of the right frontomaxillar border while the left structure shifted posteriorly. The left premaxilla was shorter and narrower compared to the longer and wider right premaxilla (Fig. 2J). Phocoenidae had the lowest landmark displacements among the Delphinoidea with frontomaxillary border shifts similar to Monodontidae, the right border moving posteriorly while the left structure shifted in the opposite direction. The posterior-most extension of maxillae shifted to the right as in Kogiidae (Fig. 2I).

The Principal Components (PC) of asymmetric shape revealed a grouping of species mainly along the first two PCs accounting for 50% of the variation – 30.1% in PC1, 19.8% in PC2 (Fig. 3; Supporting Information, Fig. S1). PC1 described the skull outline and nasal septum moving to the left while the suture between the frontals and the posterior extension of the maxillae were displaced to the right with a shortening of the right structure, and the right premaxilla showing posterior extension. Monodontidae had extremely low PC1 scores, followed by Globicephalinae and the 'river dolphins', while Physeteroidea had high scores, especially Kogiidae. PC2 mainly described a general widening of the right side of the skull by deviation of the nasal septum to the left and the frontomaxillar border to the right, along with a noticeable posterior extension and enlargement of the right premaxilla and maxilla, including displacement of the maxillae to the left side. Kogiidae, *P. macrocephalus*, Globicephalinae and Monodontidae were distributed in extreme opposite scores of the 'river dolphins', Ziphiidae and Phocoenidae.

The phylogenetic signal in the average asymmetric skull shape among species was both statistically significant using unweighted (tree length = 0.025 and $P < 0.0001$) and weighted (tree length = 0.031 and $P < 0.0001$) squared-change parsimony on rooted trees. In the morphospace mapping on phylogeny, members of the superfamily Physeteroidea were close to each other, the 'river dolphins' were also grouped, and, among Delphinoidea, Monodontidae were distant from their relatives, as were to a lesser extent Globicephalinae, whereas Phocoenidae were closer to the 'river dolphins' and Ziphiidae than to the other Delphinoidea taxa (Fig. 3; Supporting Information, Fig. S1).

In terms of the angular differences of the species-specific vectors, the quality of cranial asymmetry among the ten families of odontocetes indicated a similar general pattern, with some variation. Closely related species mostly showed more similar expressions of asymmetry than distantly related species. The families with the most divergent patterns were Kogiidae and the 'river dolphins', especially *P. blainvillei*, resulting in the greatest angular difference in the data set of 30.7° between *Kogia sima* and *P. blainvillei*, while the most acute angle within the 'river dolphins' was a difference of 4.0° between *L. vexillifer* and *P. blainvillei* (Supporting Information, Table S3). The family presenting the greatest variation in angular difference among its species was Delphinidae, in which Globicephalinae stood out, exemplified by angles of 24.1° between *Globicephala macrorhynchus* and *Sousa chinensis,* followed by 23.7° for the comparison with *Sousa plumbea* and 23.6° with *Stenella longirostris.* The smallest variation in the angular difference among Delphinidae species was 2.4° between *S. plumbea* and *S. chinensis*. The Delphininae species were very similar, showing small angular differences (2.6° between *Stenella frontalis* and *Stenella attenuata* and 2.6° between *S. frontalis* and *Tursiops aduncus,* closely followed by 2.7° between *S. attenuata* and *Stenella clymene,* 2.8° between *S. longirostris* and *Delphinus delphis,* and *2.9° between S. attenuata and D. delphis*). The family with the smallest angular differences among its species was Phocoenidae (greatest angular difference was 7.9° between *Neophocaena phocaenoides* and *Phocoenoides dalli,* smallest difference was 3.2° between *Phocoena phocoena* and *Phocoena dioptrica,* followed by 3.4° between *N. phocaenoides* and *Neophocaena asiaeorientalis*) (Supporting Information, Table S3).

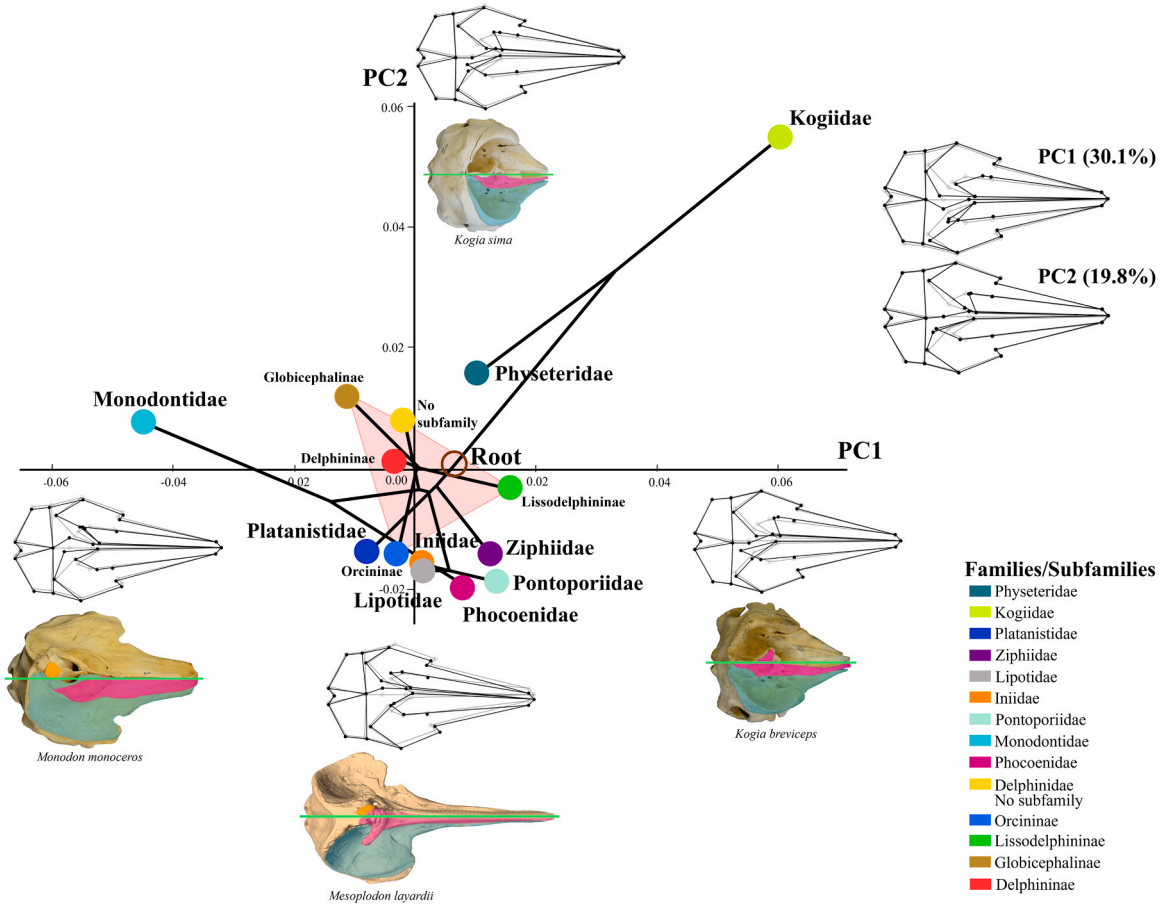

Fig. 3. Morphometric space of asymmetric average skull shape by families and subfamilies of Odontoceti along Principal Components 1 and 2 including the phylogenetic tree mapped on shape by weighted squared-change parsimony. The polygon highlights the subfamilies of Delphinidae (light red). Skull wireframes in dorsal view are showing the asymmetric components (black), overlapping with symmetric components (grey). The green straight line represents the sagittal plane between the midpoint of the rostral tip and the dorsal margin of the *foramen magnum*, the pink structure is the right premaxilla, the blue structure is the right maxilla, and the orange structure is the right nasal bone.

3.2. Magnitude of asymmetry

The wide spectrum of asymmetry magnitude of species (and one hybrid) across the ten families of odontocetes is illustrated in Fig. 4. In terms of the quantity of asymmetry, the greatest displacements were found in Kogiidae, Monodontidae and Globicephalinae, followed by Physeteridae, Platanistidae and Lipotidae, while asymmetry was lowest in Lissodelphininae, Phocoenidae, Iniidae and Pontoporiidae (Supporting Information, Fig. S2).

The superfamily Physeteroidea demonstrated the most prominent landmark displacements relative to symmetry, and the family which showed the greatest magnitudes of asymmetry was Kogiidae, with *Kogia breviceps* being the most asymmetric species, closely followed by *K. sima*. Monodontidae also showed high asymmetry, particularly *Monodon monoceros* in both sexes. We also found high levels of asymmetry in the delphinid subfamily Globicephalinae, with *G. macrorhynchus* being the most asymmetric species, followed by *Pseudorca crassidens*, *Globicephala melas*, *Grampus griseus* and *Feresa attenuata,* while *Orcaella brevirostris* and *Steno bredanensis* were the least asymmetric species of this widely variable clade, showing modest asymmetry. Other representatives of Delphinidae among the most asymmetric species were *Lagenorhynchus albirostris*, the Delphininae *Stenella coeruleoalba* and *Lagenodelphis hosei* and the Lissodelphininae *Lagenorhynchus cruciger*. The least asymmetric Delphinidae was *Sousa* sp., the least asymmetric Delphininae was *Sotalia guianensis*, and among the Lissodelphininae these were *Lagenorhynchus obscurus* and *Lagenorhynchus obliquidens*. The least asymmetric delphinoid family was Phocoenidae, with *Phocoena spinipinnis* and *P. dalli* being the most and the least asymmetric, respectively. *P. macrocephalus*, *P. gangetica*, *L. vexillifer* and the ziphiids *Mesoplodon layardii*, *Hyperoodon ampullatus* and *Ziphius cavirostris* were highly asymmetric. Intermediate values comprised some Ziphiidae (*e.g. Mesoplodon ginkgodens* and *Mesoplodon hectori),* and the remaining of Delphinidae (*e.g.* Orcininae). Other ziphiids, as well as *I. geoffrensis* and *P. blainvillei*, were among the least asymmetric species.

3.3. Asymmetry and sound production

Spearman's correlation coefficient was significant and strong between the two parameters of sound production and skull size. Source level (SL) and centroid size (CS) had a directly proportional relationship $\rho = 73.15$ ($P < 0.001$), while for centroid frequency (cF) and CS there was an even stronger correlation, with these variables presenting an inversely proportional relationship $\rho = -82.97$ ($P < 0.001$) in the principal dataset with all species, including *K. sima* and *G. macrorhynchus*. Thus, to remove latent body size effects from acoustic parameters, the residual values for each of these sound parameters from the regression on the species medians of skull CS were used for downstream analyses.

The model including SL and CS as predictor variables for asymmetry magnitude performed best (AICc = −193.30; ΔAICc = 0.00; weight AICc = 0.565; logLik = 101.33; degrees of freedom = 34) in the AICc selection with delta < 2. In addition, the model with SL as the only predictor variable was also selected (AICc = −192.8; ΔAICc = 0.52; weight AICc = 0.435; logLik = 99.79; degrees of freedom = 34).

In the best performing GLMs, SL and CS explained 33.1% of the variation in magnitude of asymmetry, with only SL as predictor being statistically significant ($P = 0.002$ for SL; $P = 0.076$ for CS; AICc = −200.25; degrees of freedom = 35). The model including only SL as predictor was statistically significant ($P = 0.002$; AICc = −199.12; degrees of freedom = 35), explaining 26.8% of the magnitude of cranial asymmetry (Fig. 5 – there is no pattern to the distribution of taxa emitting echolocation clicks using different frequencies along the magnitude of asymmetry).

Using PGLS with Pagel's λ in the selected models, SL was the only significant predictor variable in both models, including SL and CS ($\lambda = 0.916$; $P = 0.016$ for SL and $P = 0.319$ for CS), as well as SL was significant as a sole predictor variable ($\lambda = 0.852$; $P = 0.006$) (Table 3).

In the supplementary dataset excluding *K. sima* and *G. macrorhynchus*, similar correlations between CS and sound parameters were found, SL and cF having correlation coefficients of $\rho = 73.22$ ($P < 0.001$) and $\rho = -81.37$ ($P < 0.001$), respectively. The model with SL and CS performed best (AICc = −192.8; ΔAICc = 0.00; weight AICc = 0.574; logLik = 101.11; degrees of freedom = 32). Another model with delta < 2 included SL, cF and CS (AICc = −192.2; ΔAICc = 0.60; weight AICc = 0.426; logLik = 102.20; degrees of freedom = 32). In the best performing GLMs, SL was the only sound parameter consistently showing significant association with magnitude of cranial asymmetry. The model including SL and CS ($R^2 = 35.1\%$; $P = 0.002$ for SL; and

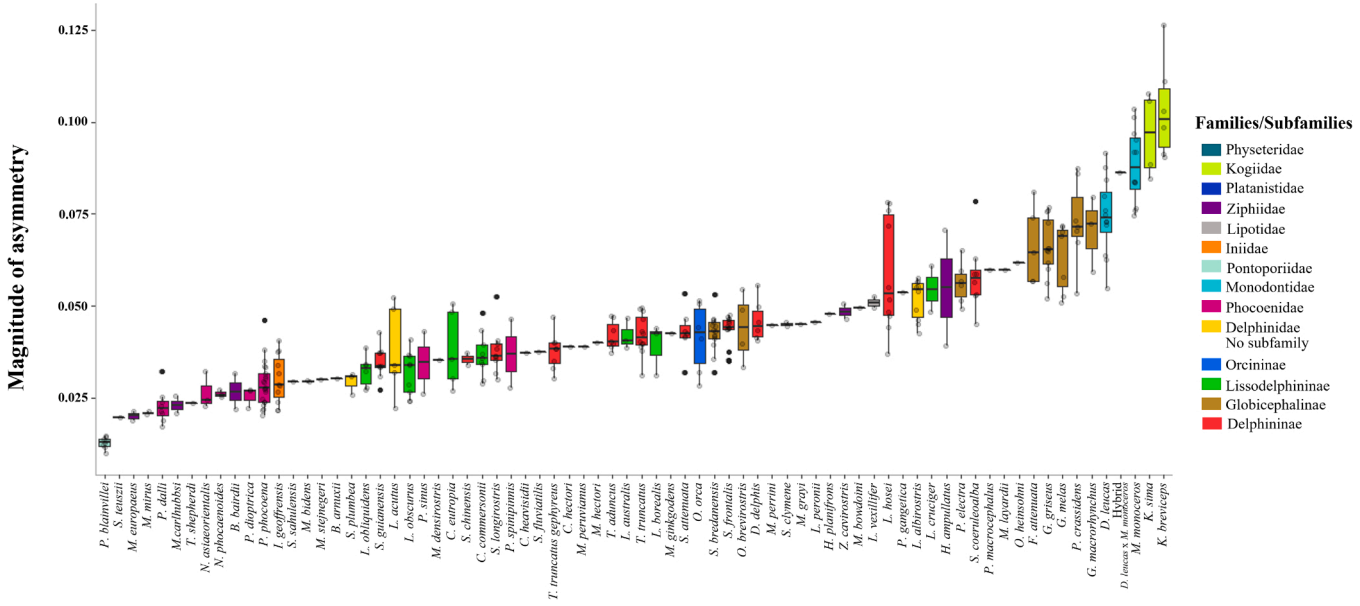

Fig. 4. Box plot of skull asymmetry magnitude for each investigated species of the suborder Odontoceti. The lower limit of the box shows the first quartile (Q1), the bold line represents the median, and the top limit is the third quartile (Q3). The vertical whiskers represent 1.5 times the interquartile range. The outliers are shown as black dots. Each specimen is represented by a grey dot.

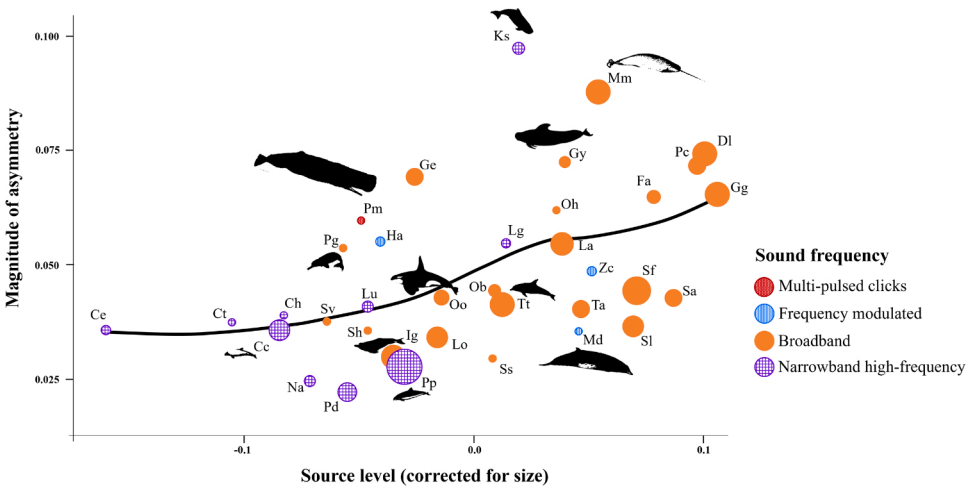

Fig. 5. Scatter plot of the partial effects from Generalized Linear Models (GLMs) showing significant association between the species-specific median of magnitude of asymmetry and residuals of a regression of source level, in decibels (dB), on centroid size (Table 2). Red circle (dotted) is species that produces multi-pulsed clicks, blue circles (vertical stripes) are species that emit frequency modulated clicks, orange circles (solid fill) are species that emit broadband clicks and purple circles (grid) are species using narrowband high-frequency clicks (Table 2). The size of the circles is proportional to the species-specific sample sizes (Supporting Information, Table S1). The black line is the sample best fit line.

Table 3
Phylogenetic Generalized Least Squares (PGLS) analysis based on the molecular phylogeny of McGowen *et al.* (2020) in selected models by second-order Akaike Information Criterion (AICc) of the variables: species-specific median of magnitude of asymmetry as response variable (Asymmetry), and as predictor variables species-specific sound parameter residual (size-corrected) source level – SL (dB re 1μPa at 1 m) and species-specific median centroid size from skull samples – CS for specimens of the suborder Odontoceti using the maximum values of sound parameters to *Kogia sima* (Malinka *et al.*, 2021) and *Globicephala macrorhynchus* (Pedersen *et al.*, 2021). Number of parameters (*df*).

Models	Lambda	*df*	Predictor Variables	Coefficient value	Standard Error	t-value	p-value
Asymmetry ~ SL+ CS	λ = 0.916	31	**SL**	**0.124**	**0.049**	**2.56**	**0.016**
			CS	-0.00003	0.00003	-1.01	0.319
Asymmetry ~ SL	λ = 0.852	31	**SL**	**0.142**	**0.047**	**2.99**	**0.006**

P = 0.022 for CS; AICc = −194.21; degrees of freedom = 32), and SL, cF and CS (R^2 = 39.4%; P = 0.026 for SL; P = 0.158 for cF; P = 0.018 for CS; AICc = −194.41; degrees of freedom = 32) were statistically significant for the predictor variables SL and CS.

Using PGLS with Pagel's λ in the selected models on the reduced dataset, only the predictor variable SL was significant in the model including SL and CS (λ = 0.913; P = 0.013 for SL; P = 0.038 for CS), and CS as predictor variable was significant for the model with SL, cF and CS (λ = 0.908; P = 0.088 for SL; P = 0.120 for cF; and P = 0.030 for CS) (Supporting Information, Table S4).

4. Discussion

4.1. Manifestations of cranial asymmetry

Asymmetric shape variation was consistent in its directionality and in the structures involved across all ten odontocete families, with the skull midline and premaxillae shifting to the left as observed by Ness (1967), Mead (1975) and Heyning (1989). The skull outline and suture crest between the frontal and interparietal were displaced to the right with concomitant greater dimensions of the right premaxilla and maxilla compared to the left (Fig. 2), in accordance with Galatius and Goodall (2016), Huggenberger *et al.* (2016a) and Laeta *et al.* (2020). The landmark at the suture between the frontals, close to the nasal bones, indicates a leftward deviation of the skull midline in this area. A similar shift of nasal bones in taxa retaining both nasals (*Physeter* only retains one nasal and *Kogia* spp. none) has been described previously (Hirose *et al.*, 2015; Huggenberger *et al.*, 2016a; Laeta *et al.*, 2020).

Mapping the asymmetric shape on phylogeny showed a clear relationship between shape and phylogeny, with related taxa generally being in proximity of each other, *e.g.* within Physeteroidea, 'river dolphins' and subfamilies of Delphinidae, along the PC1 scores (Fig. 3; Supporting Information, Fig. S1). There was also association between more distantly related taxa along the PC2 scores, *e.g.* Physeteroidea, Globicephalinae and Monodontidae, showing remarkable displacement of cranial structures, with a phenotypic similarity of asymmetry among these groups.

Greater differences in the qualitative expressions of asymmetry were mostly observed between distantly related species, *e.g. Kogia sima* and *Pontoporia blainvillei*, or for some more closely related species occurring in distinct habitats, *e.g.* coastal *Sousa chinensis* and oceanic *Lagenodelphis hosei*. Highly similar expressions mostly occurred between closely related species *e.g.*, within Ziphiidae or Phocoenidae, or between more distantly related species exploring similar strata of water, *e.g.* the deep-diving *Monodon monoceros* , *Ziphius cavirostris* and *Globicephala* spp. (Supporting Information, Table S3). Similar results were found within Delphinoidea by Laeta *et al.* (2020).

Kogiidae, Monodontidae, *Physeter macrocephalus*, and Globicephalinae were the most asymmetric taxa, followed by *Platanista gangetica* and *Lipotes vexillifer*. Lissodelphininae, Phocoenidae, *Inia geoffrensis* and *P. blainvillei*, presented the lowest levels of asymmetry, in accordance with previous studies (Fig. 4; Supporting Information, Fig. S2) (Ness, 1967; Galatius and Goodall, 2016; Huggenberger *et al.*, 2016a; Laeta *et al.*, 2020).

Phylogeny has been demonstrated to play a major role, likely because factors influencing asymmetry are shared by closely related taxa (Coombs *et al.*, 2020), as exemplified by similar habitat use and foraging patterns within many clades, *e.g.*, Physeteroidea, Ziphiidae, Monodontidae and Phocoenidae. We also identified similarities in the asymmetric shapes among closely related taxa (Supporting Information, Fig. S1), and the high Pagel's λ values in our models reinforces this strong phylogenetic signal (Table 3; Supporting Information, Table S4). Furthermore, cranial asymmetry may be driving the evolution of the interactions of cranial structures *i.e.* modularity (Churchill *et al.*, 2019). Among the earliest diverging marine taxa, the physeteroids *P. macrocephalus* and *Kogia* spp. showed the greatest levels of asymmetry, with an emphasis on posterior extension of the premaxillae. In Kogiidae, this included a remarkable displacement of the nasal septum

(Figs. 2A-B and 4; Supporting Information, Fig. S2). Some peculiarities within these species are evidenced by large differences between the vectors describing species-specific asymmetry (Supporting Information, Table S3). In Ziphiidae, the asymmetry was low for most species studied here – except for *Mesoplodon layardii*, *Hyperoodon* spp. and *Z. cavirostris*, all of which showed marked deviation of the skull midline to the left with greater dimensions of the right premaxilla as compared to the left (Figs. 2D and 4). Heyning (1989) highlighted asymmetry between the premaxillae in *Z. cavirostris*, but later studies did not find marked asymmetry throughout Ziphiidae (Hirose *et al.*, 2015; Coombs *et al.*, 2020). Coombs *et al.* (2020) attributed this low asymmetry to their selection of landmarks, which did not reflect the peculiarities of asymmetrical shape in the bone structure of this family, particularly with regard to the premaxillae. However, the present study investigated the anteroposterior premaxillary extremities, as well as the greatest width of the premaxillae, generally represented by the lateral extensions of the premaxillary crests (Fig. 1, Table 1), and although some taxa such as *Z. cavirostris* show high asymmetry, this is not the general condition in this family (Heyning, 1989; Hirose *et al.*, 2015).

Among the 'river dolphins', there is a general similarity in the quality of asymmetric shape, characterized by an anterior and lateral enlargement of the right frontomaxillar border and a left shift of the suture between frontals (Fig. 2C; 2E-G). These species showed a large range of magnitude of asymmetry, with *P. gangetica* and *L. vexillifer* highly asymmetric, while *I. geoffrensis* and, particularly, *P. blainvillei,* were the least asymmetric (Fig. 4; Supporting Information, Fig. S2). These findings agree with previous studies where *P. gangetica* was recognized as the most asymmetric 'river dolphin' and *P. blainvillei* was the least asymmetric odontocete (Ness, 1967; Huggenberger *et al.*, 2016a; Coombs *et al.*, 2020).

Within Delphinoidea, we also find large differences in the magnitude of asymmetry as reported by Ness (1967) and Yurick and Gaskin (1988). Monodontidae showed the greatest displacements, with greater dimensions of the right premaxilla and maxilla, and leftward displacement of the skull midline. Much more subtle manifestations of asymmetry occurred in Phocoenidae, which were the least asymmetric delphinoids (Figs. 2H-I and 4; Supporting Information, Fig. S2). In the Delphinidae, qualitative manifestations of asymmetry were relatively diverse with large differences between subfamilies such as Globicephalinae and Delphininae (Fig. 2J; Supporting Information, Table S3). A wide spectrum was also evident with respect to the magnitude of asymmetry, with most Globicephalinae showing high levels, approaching those of Monodontidae for some species (Fig. 4; Supporting Information, Fig. S2). Among the least asymmetric delphinids were *Sousa* spp., *Sotalia guianensis*, and the Lissodelphininae *Cephalorhynchus* sp., *Lagenorhynchus obscurus* and *Lagenorhynchus obliquidens*, overlapping with phocoenids (Fig. 4; Supporting Information, Fig. S2 and Table S3). These patterns are in agreement with previous findings (Galatius and Goodall, 2016; Huggenberger *et al.*, 2016a; Laeta *et al.*, 2020).

4.2. Cranial asymmetry and sound production

We found that the source level predicted the magnitude of asymmetry more than any other biosonar parameter, as previously suggested by Laeta *et al.* (2020) (Fig. 5; Table 2). Asymmetry has previously been widely hypothesized to be associated with sound frequency (since Cranford *et al.*, 1996), but neither Galatius and Goodall (2016) nor Huggenberger *et al.* (2016a) found such a relationship. Frequency only occurred in one of the selected models for the dataset excluding *K. sima* and *Globicephala macrorhynchus*, whereas source level and centroid size occurred much more prominently, with source level also occurring in the model including frequency. In the more complex model including all the predictor variables – source level, frequency and centroid size, only frequency was not significant ($P = 0.026$ for SL; $P = 0.158$ for cF; $P = 0.018$ for CS). As frequency is related to the size of the sound-producing apparatus (Jakobsen *et al.*, 2013; Jensen *et al.*, 2018), it is not surprising that it is among the selected models to explain asymmetry. This variable can be a way to adapt the size of the sound producing apparatus in animals with suggested unilateral sound production to echolocation clicks (Madsen *et al.*, 2010, 2013; Ames *et al.*, 2020), even if it is not a predictor of cranial asymmetry. As for the increasing source level, it may enable odontocetes to detect prey at long distances through scanning larger volumes in deep waters (Table 2). Higher source level may be attained by hypertrophy of the right sound production organs at the expense of the left size. These relationships across all odontocetes are similar to those found within Delphinoidea (Laeta *et al.* 2020). They are further aligned with Jensen *et al.*'s (2018) proposal that increased cranial asymmetry may be related to the general evolutionary hyperallometric development of large sound production structures in large odontocetes. Both the hypertrophy of the sound producing structures and the asymmetry can contribute to the production of high biosonar signal output, allowing greater volumes of water to be scanned by echolocation. Furthermore, Foskolos *et al.* (2019) found that larger (but still very small) volumes of air are used by the largest sound-generating structures on the right under the need to produce clicks as depth increases. This may be another factor associating depth, the size of the sound producing apparatus, and hence asymmetry, as odontocetes are generally expected to have unilateral click production on the right side (Madsen *et al.*, 2010, 2013; Ames *et al.*, 2020).

The lateralized production of echolocation clicks (Madsen *et al.* 2010, 2013; Ames *et al.*, 2020) is consistent with the enlargement of bone structures on the right side (Galatius and Goodall, 2016; Huggenberger *et al.*, 2016a; Laeta *et al.*, 2020). This suggests functionality of the cranial asymmetry in relation to support of larger soft tissue organs on the right side – the nasal apparatus, melon and related muscular complex (Schenkkan, 1973; Heyning and Mead, 1990; Cranford, 1996). The magnitude of asymmetry, as well as its most important predictors found here, skull size and higher source level, are all subject to ontogenetic development. The cranial facial and rostral development (Sydney, 2010; Galatius *et al.*, 2011; Del Castillo *et al.*, 2017) and the maturation of sound-generating structures (Frainer *et al.*, 2015; 2019), may be important for shaping biosonar signal properties *e.g.* enabling emission of more complex sounds and higher source level (Jensen *et al.*, 2018). However, it is still unclear how such functional changes to sound-generating structures may drive the observed increase in asymmetry during ontogeny (Sydney, 2010; Lanzetti *et al.*, 2022).

Thus, our results imply that greater levels of asymmetry are related to hypertrophy of sound-generating structures on the right side, especially among taxa that use deep pelagic waters, represented by extreme cases such as physeteroids, monodontids and globicephalines. These species emit powerful echolocation clicks with peak-to-peak source level around 196–240 dB re 1μPa (Fig. 5; Table 2), enabling them to scan large volumes of water at great depths to locate prey in low densities over long distances. The range capability of such sounds to penetrate further increases the chance that there is sufficient energy for the echo to retain relevant information to be decoded after reaching a target (Au, 2018). However, we did not observe a generalized high asymmetry among deep-diving ziphiids, which also use loud sounds 203–214 dB re 1μPa (Fig. 5; Table 2). It is likely that there is some noise in our source level dataset, as an accurate measurement of this parameter requires an on-axis recording and this can be difficult for deep-diving species that might not use maximum biosonar outputs near the surface. Thus, there are likely several underestimates in the dataset, particularly for species with few recordings. Such noise may have caused our models to underestimate this relationship of asymmetry and source level.

The ability of deep-diving odontocetes to emit powerful sounds was critical to their evolutionary success in deep water ecological niches (Jensen *et al.*, 2018; Foskolos *et al.*, 2019; Madsen *et al.*, 2023; Table 2). However, adaptations for the accommodation of large sound generating structures can also involve aspects of cranial morphology other than asymmetry (Churchill *et al.*, 2018). For example, it has been suggested that the deeper cranial concavity of the facial region found in pelagic

phocoenids relative to coastal relatives allows larger sound-generating structures (Galatius *et al.*, 2011). Concavity as a potential adaption for accommodating a large sound producing apparatus is repeated in the delphinid subfamily Lissodelphininae, particularly in *Lagenorhynchus cruciger*, which is also remarkably asymmetric compared to its close relatives (Galatius and Goodall, 2016; Del Castillo *et al.*, 2017; Laeta *et al.*, 2020). This may be the case for some ziphiids such as *Mesoplodon* sp., which show widespread low asymmetry while having very concave facial profiles that may alleviate the need for a higher degree of asymmetry. Among fossil ziphiids, elevation of the cranial vertex has previously been proposed to be associated with adaptation of echolocation for deep diving (Bianucci *et al.*, 2016). Furthermore, among extant ziphiids, the greater concavity of the facial region has been proposed to be associated with biosonar adaptations to a deep-diving lifestyle (Vicari *et al.*, 2023). Both elevation of the vertex and increased facial concavity would facilitate accommodation of a larger sound producing apparatus, analogous to the increased directional asymmetry favouring the click-producing side in odontocetes with lateralized click production. The vertex elevation observed among the very asymmetric *Physeter macrocephalus* and Kogiidae (Ness, 1967; Heyning and Mead, 1990) may be another reflection of this adaptation, indicating that it has occurred convergently across Odontoceti. Vertex elevation and deep concavity of the facial region were also observed in stem and crown extinct physeteroids (Velez-Juarbe *et al.*, 2015; Lambert *et al.*, 2017), including taxa with high cranial asymmetry, *Orycterocetus* and *Aulophyseter* (Coombs *et al.*, 2020). Despite the potential functionality of such cranial shapes for the production of more powerful sounds, relationships to specific habitats such as deep waters have not been established among these fossils (Lambert *et al.*, 2017).

Platanista gangetica and *Lipotes vexillifer*, which are certainly not deep divers, showed relatively high levels of asymmetry. Both species live (or lived, as *L. vexillifer* is now considered extinct) in turbid rivers and have reduced vision, particularly *P. gangetica* (Herald *et al.*, 1969; Zhou, 2009; Thewissen, 2009; Fig. 4; Supporting Information, Fig. S2). These taxa may have strategies to optimize sound production, even though they do not emit comparatively loud sounds (183 dB re 1μPa for *P. gangetica*; Fig. 5; Table 2), and *L. vexillifer* has also been described with strong asymmetry in the facial soft tissues (Hinton, 1936).

In the evolutionary history of odontocetes, echolocation has evolved as an essential sensory modality (Geisler *et al.*, 2014; Boessenecker *et al.*, 2017). The relationship between cranial asymmetry and the production of powerful sounds via hypertrophy of nasal structures on the right side as proposed by Laeta *et al.* (2020) for Delphinoidea was corroborated here for all ten families of odontocetes with a phylogenetic signal in both qualitative variation and quantitative asymmetry. Across toothed whales, evolutionary models have shown that the magnitude of asymmetry was partially explained by source level so that animals producing larger source levels tend to have higher cranial asymmetry. This suggests that the unique asymmetry found in odontocete skulls is related to morphological adaptations that allow for larger investment in a biosonar sound generator, allowing them to detect prey at longer ranges. Where similarities in the magnitude of asymmetry are manifested in more distantly related taxa, there is likely an evolutionary convergence of asymmetry as an adaptation to allow production of loud sounds. However, a substantial part of the variation was not explained in our models. This may be due to other factors contributing to asymmetry, such as the complex interaction with other anatomical adaptations (*e.g.*, concavity and allometry) related to the enlargement of the sound production apparatus, and to incomplete data on species-specific maximum source levels. The general similarity of expressions of asymmetry implies that it serves the same function throughout Odontoceti and is a shared derived character. With the data currently available, we cannot address the functional implications of the qualitative variation. Further light could be shed on these issues by the inclusion of fossil species, or more accurate and extensive data on sound parameters and ecology of the species.

CRediT authorship contribution statement

The preparation and submission of this original version of the manuscript was authorized by all authors, with the following contributions: M. Laeta & A. Galatius conceived the study; M. Laeta acquired the database of digital images with the support of J.A. Oliveira, O. Lambert & A. Galatius; M. Laeta & A. Galatius performed the analyses and interpreted the results. M. Laeta & A. Galatius wrote the original manuscript, with contributions from J.A. Oliveira, S. Siciliano, O. Lambert & F.H. Jensen.

Declaration of competing interest

The authors declare that they have no known competing financial interests or personal relationships that could have appeared to influence the work reported in this paper.

Data Availability

Data are available in landmark format upon request.

Acknowledgements

We thank Greicy Ruenes of the Universidade Estadual do Norte Fluminense Darcy Ribeiro (UENF), Rio de Janeiro, Brazil for supporting parts of database of digital images. We thank Morten Tange Olsen and Daniel Klingberg Johansson of the Natural History Museum of Denmark (NHMDK) and Richard Sabin of the Natural History Museum, London, UK (NHMUK) for assistance during the visit to their respective collections, Jean-Marc Lorphelin, Philippe Somma, Fatiha Boumalk, and Lyse Jokiel of the Centre d'Imagerie Médicale de Bois-Bernard for the CT-scans of the specimens from the Muséum national d'Histoire naturelle, France (MNHN-France), and Cristian Becker, Jhoann Luis Canto Hernandez and Reynaldo Montenegro of the Museo Nacional de Historia Natural/National Museum of Natural History, Chile (MNHN-Chile), Simone Farina of the Museo di Storia Naturale dell'Università di Pisa/Natural History Museum of the University of Pisa, Italy (MSNUP), Felix G. Marx of the Museum of New Zealand Te Papa Tongarewa, New Zeland (Te Papa), Maureen Flannery and Arya Natarajan of the California Academy of Sciences, United States of America (CAS:MAM), Verity L. Mathis & Edward Stanley of the Florida Museum of Natural History, United States of America (UF-Mammals), Michael McGowen & Janine Hinton of the National Museum of Natural History, Smithsonian Institution, United States of America (USNM), Philip Unitt of San Diego Natural History Museum, United States of America (SDNHM), Matthew Gibson & Morgan Churchill of The Charleston Museum, United States of America (ChM) and Aren Gunderson & Link Olson of the Mammal Collection at the University of Alaska Museum of the North, United States of America (UAM:Mamm) for providing digital images and information from their databases. Collection members of the Museu Nacional/Universidade Federal do Rio de Janeiro, Brazil (MN/UFRJ), Grupo de Estudos de Mamíferos Marinhos do Rio Grande do Sul, Brazil (GEMARS) and Muséum national d'Histoire naturelle, France (MNHN-France) helped at these institutions. M.L. was awarded a 'Small Grant in Aid of Research' by the Society for Marine Mammalogy (2016 & 2017), and by the Coordenação de Aperfeiçoamento de Pessoal de Nível Superior (CAPES/Brazil) (PDSE - 88881.190612/2018-01). We thank Jonathan Geisler and an anonymous reviewer for their constructive comments that helped improving the manuscript.

Appendix A. Supporting information

Supplementary data associated with this article can be found in the online version at doi:10.1016/j.zool.2023.126108.

References

Adams, D., Collyer, M., Kaliontzopoulou, A., 2020. Geomorph: geometric morphometric analyses of 2D/3D landmark data. R Package version 3.2.0. Available at: ⟨https://CRAN.R-project.org/package=geomorph⟩.

Aguilar Soto, N., Johnson, M.P., Madsen, P.T., Díaz, F., Domínguez, I., Brito, A., Tyack, P., 2008. Cheetahs of the deep sea: deep foraging sprints in short-finned pilot whales off Tenerife (Canary Islands). J. Anim. Ecol. 77, 936–947.

Amaral, K.B., Danilewicz, D., Zerbini, A., Di Beneditto, A.P., Andriolo, A., Alvares, D.J., Secchi, E., Ferreira, E., Sucunza, F., Borges-Martins, M., Santos, M.C.O., Cremer, M., Denuncio, P., Ott, P.H., Moreno, I.B., 2018. Reassessment of the franciscana *Pontoporia blainvillei* (Gervais & d'Orbigny, 1844) distribution and niche characteristics in Brazil. J. Exp. Mar. Biol. Ecol. 508, 1–12.

Ames, A.E., Beedholm, K., Madsen, P.T., 2020. Lateralized sound production in the beluga whale (*Delphinapterus leucas)*. J. Exp. Biol. 223, jeb2263316.

Amorim, P.H.J., Moraes, T.F., Silva, J.V.L., Pedrini, H., 2015. InVesalius: an interactive rendering framework for health care support. 11th International Symposium on Visual Computing (ISVC). Springer-Verlag, Las Vegas, NV, pp. 45–54.

Arnqvist, G., Mårtensson, T., 1998. Measurement error in geometric morphometrics: empirical strategies to assess and reduce its impact on measures of shape. Acta Zool. Acad. Sci. Hung. 44, 73–96.

Arvy, L., 1977. Asymmetry in cetaceans. Investig. Cetacea 8, 161–212.

Au, W.W.L., 2018. Echolocation. In: Würsig, B., Thewissen, J.G.M., Kovacs, K. (Eds.), Encyclopedia of Marine Mammals, third ed. Academic Press, London, pp. 289–299.

Au, W.W.L., Penner, R.H., Turl, C.W., 1987. Propagation of beluga echolocation signals. J. Acoust. Soc. Am. 82, 807–813.

Azevedo, A.F., Oliveira, A.M., Viana, S.C., Van Sluys, M., 2007. Habitat use by marine tucuxis (*Sotalia guianensis*) (Cetacea: Delphinidae) in Guanabara Bay, south-eastern Brazil. J. Mar. Biol. Assoc. U. Kingd. 87, 201–205.

Baird, R.W., Ligon, A.D., Hooker, S.K., Gorgone, A.M., 2001. Subsurface and nighttime behaviour of pantropical spotted dolphins in Hawai'i. Can. J. Zool. 79, 988–996.

Baird, R.W., Jarvis, S.M., Webster, D.L., Rone, B.K., Shaffer, J.A., Mahaffy, S.D., Gorgone, A.M., Moretti, D.J., 2014. Odontocete studies on the pacific missile range facility in July/August 2013: satellite-tagging, photo-identification, and passive acoustic monitoring, 2014. U.S. Pacific Fleet, NAVFAC PAC - HDR Environmental, Operations and Construction, Inc.,, Olympia.

Baker, A.N., 1981. The southern right whale dolphin *Lissodelphis peronii* (Lacépède) in Australasian waters. Natl. Mus. N. Zeal. Rec. 2, 17–34.

Bartón, K., 2020. Mu-MIn: multi-model inference. R Package version 1.43.17. Available at: ⟨https://CRAN.R-project.org/package=MuMIn⟩.

Beddard, F.E., 1900. A book of whales. G. P. Putnam's Sons, New York, NY and John Murray, London.

Bernasconi, M., Nøttestad, L., Axelsen, B.E., Krakstad, J.O., 2011. Acoustic observations of dusky dolphins *Lagenorhynchus obscurus* hunting cape horse mackerel *Trachurus capensis* off Namibia. Mar. Ecol. Prog. Ser. 429, 209–218.

Best, P.B., 1999. Food and feeding of sperm whales *Physeter macrocephalus* off the west coast of South Africa. S. Afr. J. Mar. Sci. 21 (1), 393–413.

Bianucci, G., di Celma, C., Urbina, M., Lambert, O., 2016. New beaked whales from the late Miocene of Peru and evidence for convergent evolution in stem and crown Ziphiidae (Cetacea, Odontoceti). PeerJ 4, e2479.

Black, N.A., 1994. Behavior and ecology of Pacific white-sided dolphins (*Lagenorhynchus obliquidens*) in Monterey Bay, California. Master thesis. San Francisco State University,.

Boessenecker, R.W.E., Ahmed, E., Geisler, J.H., 2017. New records of the dolphin *Albertocetus meffordorum* (Odontoceti: Xenorophidae) from the lower Oligocene of South Carolina: encephalization, sensory anatomy, postcranial morphology, and ontogeny of early odontocetes. PLoS One 12, e0186476.

Bookstein, F.L., 1991. Morphometric tools for landmark data: geometry and biology. Cambridge University Press, Cambridge.

Bräger, S., Bräger, Z., 2018. Range utilization and movement patterns of coastal Hector's dolphins (*Cephalorhynchus hectori*). Aquat. Mamm. 44, 633–642.

Burnham, K.P., Anderson, D.R., 2002. Model selection and multimodel inference: a practical information-theoretic approach, second ed. Springer, New York, NY.

Burnham, K.P., Anderson, D.R., Huyvaert, K.P., 2011. AIC model selection and multimodel inference in behavioral ecology: some background, observations, and comparisons. Behav. Ecol. Sociobiol. 65, 23–35.

Cholewiak, D., Baumann-Pickering, S., van Parijs, S., 2013. Description of sounds associated with Sowerby's beaked whales (*Mesoplodon bidens*) in the western North Atlantic Ocean. J. Acoust. Soc. Am. 134, 3905–3912.

Churchill, M., Geisler, J.H., Beatty, B.L., Goswami, A., 2018. Evolution of cranial telescoping in echolocating whales (Cetacea: Odontoceti). Evol 72, 1092–1108.

Churchill, M., Miguel, J., Beatty, B.L., Goswami, A., Geisler, J.H., 2019. Asymmetry drives modularity of the skull in the common dolphin (*Delphinus delphis*). Biol. J. Linn. Soc. 126, 225–239.

Community, B.O, 2018. Blender - a 3D modelling and rendering package version 2.92. Stichting Blender Foundation, Amsterdam (Available at). ⟨http://www.blender.org⟩.

Coombs, E.J., Clavel, J., Park, T., Churchill, M., Goswami, A., 2020. Wonky whales: the evolution of cranial asymmetry in cetaceans. BMC Biol. 18, 86.

Cranford, T.W., Amundin, M., Norris, K.S., 1996. Functional morphology and homology in the odontocete nasal complex: implications for sound generation. J. Morph 228, 223–285.

Crespo, E.A., 2009. Franciscana dolphin *Pontoporia blainvillei*. In: Perrin, W.P., Würsig, B., Thewissen, J.G.M. (Eds.), Encyclopedia of Marine Mammals, second ed. Academic Press, San Diego, California, pp. 466–469.

Dalebout, M.L., Mead, J.G., Baker, C.S., Baker, A.N., van Helden, A.L., 2002. A new species of beaked whale *Mesoplodon perrini* sp. N. (Cetacea: Ziphiidae) discovered through phylogenetic analyses of mitochondrial DNA sequences. Mar. Mamm. Sci. 18, 577–608.

Danilewicz, D., Secchi, E., Ott, P., Moreno, I., Bassoi, M., Borges-Martins, M., 2009. Habitat use patterns of franciscana dolphins (*Pontoporia blainvillei*) off southern Brazil in relation to water depth. J. Mar. Biol. Assoc. U. Kingd. Camb. 89, 943–949.

Davis, R.W., Worthy, G.A.J., Würsig, B., Lynn, S.K., 1996. Diving behavior and at-sea movements of an Atlantic spotted dolphin in the Gulf of Mexico. Mar. Mam. Sci. 12, 569–581.

Dawson, S.M., 2018. *Cephalorhynchus* dolphins – *C. heavisidii*, *C.* eutropia, C. hectori, and C. commersonii. In: Würsig, B., Thewissen, J.G.M., Kovacs, K. (Eds.), Encyclopedia of Marine Mammals. Academic Press, London, pp. 166–172.

Del Castillo, D.L., Viglino, M., Flores, D.A., Cappozzo, H.L., 2017. Skull ontogeny and modularity in two species of *Lagenorhynchus*: morphological and ecological implications. J. Morph 278, 203–214.

de Freitas, M., Jensen, F.H., Tyne, J., Bejder, L., Madsen, P.T., 2015. Echolocation parameters of Australian humpback dolphins (*Sousa sahulensis*) and Indo-Pacific bottlenose dolphins (*Tursiops aduncus*) in the wild. J. Acoust. Soc. Am. 137, 3033–3041.

de Freitas, M., Smith, J.N., Jensen, F.H., Beedholm, K., Madsen, P.T., 2018. Echolocation click source parameters of Australian snubfin dolphins (*Orcaella heinsohni*). J. Acoust. Soc. Am. 143, 2564–2569.

Dolar, M.L.L., Walker, W.A., Kooyman, G.L., Perrin, W.F., 2003. Comparative feeding ecology of spinner dolphins (*Stenella longirostris*) and Fraser's dolphins (*Lagenodelphis hosei*) in the Sulu Sea. Mar. Mamm. Sci. 19, 1–19.

Donnelly, D., Ensor, P., Gill, P., Clark, R., Evans, K., Double, M., Webster, T., Rayment, W., Schmitt, N., 2018. New diagnostics descriptions and distribution information for Shepherd's beaked whale (*Tasmacetus shepherdi*) off southern Australia and New Zealand. Mar. Mamm. Sci. 34, 829–840.

Dryden, I.L., Mardia, K.V., 1998. Statistical Shape Analysis with Applications in R. Wiley, Chichester.

Eskesen, I.G., Wahlberg, M., Simon, M., Larsen, O.N., 2011. Comparison of echolocation clicks from geographically sympatric killer whales and long finned pilot whales (L). J. Acoust. Soc. Am. 130, 9–12.

Fahlke, J.M., Hampe, O., 2015. Cranial symmetry in baleen whales (Cetacea, Mysticeti) and the occurrence of cranial asymmetry throughout cetacean evolution. Sci. Nat. 102, 58.

Fahlke, J.M., Gingerich, P.D., Welsh, R.C., Wood, A.R., 2011. Cranial asymmetry in Eocene archaeocete whales and the evolution of directional hearing in water. Proc. Natl. Acad. Sci. U. S. A. 108, 14545–14548.

Fahlman, A., Tyson Moore, R.B., Stone, R., Sweeney, J., Trainor, R.F., Barleycorn, A.A., McHugh, K., Allen, J.B., Wells, R.S., 2023. Deep diving by offshore bottlenose dolphins (*Tursiops* spp.). Mar. Mamm. Sci. 1–16.

Fang, L., Li, S., Wang, K., Wang, Z., Shi, W., Wang, D., 2015. Echolocation signals of free-ranging Indo-Pacific humpback dolphins (*Sousa chinensis*) in Sanniang Bay, China. J. Acoust. Soc. Am. 138, 1346–1352.

Fitch, J., Brownell, R., 1968. Fish otoliths in cetacean stomachs and their importance in interpreting feeding habits. J. Fish. Res. Board Can. 25, 2561–2574.

Fordyce, R.E., 1994. *Waipatia maerewhenua*, new genus and new species (Waipatiidae, new family), an archaic Late Oligocene dolphin (Cetacea: Odontoceti: Platanistoidea) from New Zealand. In: Berta, A.; Deméré, T.A. (Eds.), Contributions in marine mammal paleontology honoring Frank C. Whitmore Jr. Proceedings of the San Diego Museum of Natural History, San Diego 29. 47–176.

Fordyce, R.E., 2002. *Simocetus rayi* (Odontoceti: Simocetidae, new family): a bizarre new archaic Oligocene dolphin from the eastern North Pacific. Smithson. Contrib. Paleobiol. 93, 185–222.

Foskolos, I., Aguilar Soto, N., Madsen, P.T., Johnson, M., 2019. Deep-diving pilot whales make cheap, but powerful, echolocation clicks with 50 μL of air. Sci. Rep. 9, 15720.

Frainer, G., Huggenberger, S., Moreno, I.B., 2015. Postnatal development of franciscana's (*Pontoporia blainvillei*) biosonar relevant structures with potential implications for function, life history, and bycatch. Mar. Mamm. Sci. 31, 1193–1212.

Frainer, G., Moreno, I.B., Serpa, N., Galatius, A., Wiedermann, D., Huggenberger, S., 2019. Ontogeny and evolution of the sound-generating structures in the infraorder Delphinida (Odontoceti: Delphinida). Biol. J. Linn. Soc. 128, 700–724.

Galatius, A., 2005. Bilateral directional asymmetry of the appendicular skeleton of the harbor porpoise (*Phocoena phocoena*). Mar. Mamm. Sci. 21, 401–410.

Galatius, A., 2006. Directional bilateral asymmetry of the appendicular skeleton of the white-beaked dolphin (*Lagenorhynchus albirostris*). Aquat. Mamm. 32, 232–235.

Galatius, A., Goodall, R.N., 2016. Skull shapes of the Lissodelphininae: radiation, adaptation and asymmetry. J. Morph 277, 776–785.

Galatius, A., Kinze, C.C., 2016. *Lagenorhynchus albirostris* (Cetacea: Delphinidae). Mamm. Species 48, 35–47.

Galatius, A., Berta, A., Frandsen, M.S., Goodall, R.N.P., 2011. Interspecific variation of ontogeny and skull shape among porpoises (Phocoenidae). J. Morph 272, 136–148.

Galatius, A., Morten, T.O., Steeman, M.E., Racicot, R.A., Bradshaw, C.D., Kyhn, L.A., Miller, L.A., 2019. Raising your voice: evolution of narrow-band high-frequency signals in toothed whales (Odontoceti). Biol. J. Linn. Soc. 126, 213–224.

Geisler, J.H., Colbert, M.W., Carew, J.L., 2014. A new fossil species supports an early origin for toothed whale echolocation. Nature 508, 383–386.

Gómez-Campos, E., Aguilar, A., Goodall, R.N.P., 2010. Serrated flippers and directional asymmetry in the appendicular skeleton of the Commerson's dolphin (*Cephalorhynchus commersonii*). Anat. Rec. 293, 1816–1824.

Goodall, R.N.P., 2009. Peale's dolphin *Lagenorhynchus australis*. In: Perrin, W.P., Würsig, B., Thewissen, J.G.M. (Eds.), Encyclopedia of Marine Mammals, second ed. Academic Press, San Diego, California, pp. 844–847.

Gopal, K., Elwen, S., Plön, S., 2016. A conservation assessment of *Cephalorhynchus heavisidii*. In: Child, M.F., Roxburgh, L., Do Linh San, E., Raimondo, D., Davies-

Mostert, H.T. (Eds.), The Red List of Mammals of South Africa, Swaziland and Lesotho. South African National Biodiversity Institute and Endangered Wildlife Trust, South Africa, pp. 1–7.
Goswami, A., 2015. Phenome10K: a free online repository for 3-D scans of biological and palaeontological specimens. Available at: ⟨www.phenome10k.org⟩.
Götz, T., Antunes, R., Heinrich, S., 2010. Echolocation clicks of free-ranging Chilean dolphins (*Cephalorhynchus eutropia*.). J. Acoust. Soc. Am. 128, 563–566.
Hanson, M., Baird, R., 1998. Dall's porpoise reactions to tagging attempts using a remotely-deployed suction-cup tag. Mar. Technol. Soc. J. 32, 18–23.
Heide-Jørgensen, M.P., Bloch, D., Stefansson, E., Mikkelsen, B., Ofstad, L.H., Dietz, R., 2002. Diving behaviour of long-finned pilot whales *Globicephala melas* around the Faroe Islands. Wildl. Biol 8, 307–313.
Herald, E.S., Brownell Jr., R.L., Frye, F.L., Morris, E.J., Evans, W.E., Scott, A.B., 1969. Blind river dolphin: first side-swimming cetacean. Sci 166, 1408–1410.
Heyning, J.E., 1989. Comparative facial anatomy of beaked whales (Ziphiidae) and a systematic revision among the families of extant Odontoceti. Contrib. Sci. 405, 1–64.
Heyning, J.E., Mead, J.G., 1990. Evolution of the nasal anatomy of cetaceans. In: Thomas, J.A., Kastelein, R.A. (Eds.), Sensory Abilities of Cetaceans. Springer, Boston, MA, pp. 67–79.
Hinton, M.A.C., 1936. Some interesting points in the anatomy of the freshwater dolphin *Lipotes* and its allies. Proc. Linn. Soc. Lond. 148, 183–185.
Hirose, A., Nakamura, G., Kato, H., 2015. Some aspects on an asymmetry of nasal bones in toothed whales. Mammal. Study 40, 101–108.
Huggenberger, S., Leidenberger, S., Oelschläger, H.H.A., 2016a. Asymmetry of the nasofacial skull in toothed whales (Odontoceti) (Available at). J. Zool.. https://doi.org/10.1111/jzo.12425.
Huggenberger, S., André, M., Oelschläger, H.H.A., 2016b. The nose of the sperm whale: overviews of functional design, structural homologies and evolution. J. Mar. Biol. Assoc. U. K. 96, 783–806.
Ichishima, H., 1994. A new fossil kentriodontid dolphin (Cetacea; Kentriodontidae) from the Middle Miocene Takinoue Formation, Hokkaido, Japan. Isl. Arc 3, 473–485.
Ichishima, H., Barnes, L.G., Fordyce, R.E., Kimura, M., Bohaska, D.J., 1994. A review of kentriodontine dolphins (Cetacea; Delphinoidea; Kentriodontidae): systematics and biogeography. Isl. Arc 3, 486–492.
Iñíguez, M.A., Tossenberger, V.P., 2007. Commerson's Dolphins (*Cephalorhynchus commersonii*) off Ría Deseado, Patagonia, Argentina. Aquat. Mamm. 33, 276–285.
Jakobsen, L., Ratcliffe, J.M., Surlykke, A., 2013. Convergent acoustic field of view in echolocating bats. Nature 493, 93–96.
Jefferson, T.A., Moore, J.E., 2020. Abundance and trends of Indo-Pacific finless porpoises (*Neophocaena phocaenoides*) in Hong Kong Waters, 1996–2019. Front. Mar. Sci. 7, 574381.
Jefferson, T.A., Leatherwood, S., Webber, M.A., 1993. FAO Species Identification Guide - marine mammals of the world. Food and Agriculture Organization of the United Nations, Rome.
Jefferson, T.A., Webber, M.A., Pitman, R.L., 2008. Marine Mammals of the World: a comprehensive guide to their identification. Academic Press, San Diego.
Jefferson, T.A., Webber, M.A., Pitman, R.L., 2015. Marine Mammals of the World: a comprehensive guide to their identification, second ed. Academic Press, San Diego.
Jensen, F.H., Rocco, A., Mansur, R.M., Smith, B.D., Janik, V.M., Madsen, P.T., 2013. Clicking in shallow rivers: short-range echolocation of Irrawaddy and Ganges River dolphins in a shallow, acoustically complex habitat. PLoS One 8, e59284.
Jensen, F.H., Wahlberg, M., Beedholm, K., Johnson, M., Aguilar Soto, N., Madsen, P.T., 2015. Single-click beam patterns suggest dynamic changes to the field of view of echolocating Atlantic spotted dolphins (*Stenella frontalis*) in the wild. J. Exp. Biol. 218, 1314–1324.
Jensen, F.H., Johnson, M., Ladegaard, M., Wisniewska, D.M., Madsen, P.T., 2018. Narrow acoustic field of view drives frequency scaling in toothed whale biosonar. Curr. Biol. 28, 3878–3885.
Joyce, T.W., Durban, J.W., Claridge, D.E., Dunn, C.A., Fearnbach, H., Parsons, K.M., Andrews, R.D., Ballance, L.T., 2017. Physiological, morphological, and ecological tradeoffs influence vertical habitat use of deep-diving toothed-whales in the Bahamas. PLoS One 12, e0185113.
Kiani, M.S., Van Waerebeek, K., 2015. A review of the status of the Indian ocean humpback dolphin (*Sousa plumbea*) in Pakistan. In: Jefferson, T.A., Curry, B.E. (Eds.), Advance in Marine Biology. Humpback dolphins (*Sousa* spp.): current status and conservation. Academic Press, Oxford, pp. 201–228.
Kim, H.Y., 2013. Statistical notes for clinical researchers – evaluation of measurement error 2: Dahlberg's error, Bland-Altman method, and Kappa coefficient. Restor. Dent. Endod. 38, 182–185.
Klingenberg, C.P., 2011. MorphoJ: an integrated software package for geometric morphometrics. Mol. Ecol. Resour. 11, 353–357.
Klingenberg, C.P., Gidaszewski, N.A., 2010. Testing and quantifying phylogenetic signals and homoplasy in morphometric data. Syst. Biol. 59, 245–261.
Klingenberg, C.P., McIntyre, G.S., 1998. Geometric morphometrics of developmental instability: analyzing patterns of fluctuating asymmetry with Procrustes methods. Evol 52, 1363–1375.
Klingenberg, C.P., Barluenga, M., Meyer, A., 2002. Shape analysis of symmetric structures: quantifying variation among individuals and asymmetry. Evol 56, 1909–1920.
Kyhn, L.A., Tougaard, J., Jensen, F., Wahlberg, M., Stone, G., Yoshinaga, A., Beedholm, K., Madsen, P.T., 2009. Feeding at a high pitch: source parameters of narrow band, high-frequency clicks from echolocating off-shore hourglass dolphins and coastal Hector's dolphins. J. Acoust. Soc. Am. 125, 1783–1791.
Kyhn, L.A., Jensen, F.H., Beedholm, K., Tougaard, J., Hansen, M., Madsen, P.T., 2010. Echolocation in sympatric Peale's dolphins (*Lagenorhynchus australis*) and Commerson's dolphins (*Cephalorhynchus commersonii*) producing narrowband high-frequency clicks. J. Exp. Biol. 213, 1940–1949.
Kyhn, L.A., Tougaard, J., Beedholm, K., Jensen, F.H., Ashe, E., Williams, R., Madsen, P. T., 2013. Clicking in a killer whale habitat: narrow-band, high-frequency biosonar clicks of harbour porpoise (*Phocoena phocoena*) and Dall's porpoise (*Phocoenoides dalli*). PLoS One 8, e63763.
Ladegaard, M., Jensen, F.H., de Freitas, M., da Silva, V.M.F., Madsen, P.T., 2015. Amazon river dolphins (*Inia geoffrensis*) use a high-frequency short-range biosonar. J. Exp. Biol. 218, 3091–3101.
Laeta, M., Ruenes, G.F., Siciliano, S., Oliveira, J.A., Galatius, A., 2020. Variation in cranial asymmetry among the Delphinoidea (Available at). Biol. J. Linn. Soc.. https://doi.org/10.1093/biolinnean/blaa161.
Laidre, K.L., Heide-Jørgensen, M.P., Dietz, R., Hobbs, R.C., Jørgensen, O.A., 2003. Deep-diving by narwhals *Monodon monoceros*: differences in foraging behavior between wintering areas? Mar. Ecol. Prog. Ser. 261, 269–281.
Lambert, O., Bianucci, G., de Muizon, C., 2017. Macroraptorial sperm whales (Cetacea, Odontoceti, Physeteroidea) from the Miocene of Peru. Zool. J. Linn. Soc. 179, 404–474.
Lanzetti, A., Coombs, E.J., Portela, M.R., Fernandez, V., Goswami, A., 2022. The ontogeny of asymmetry in echolocating whales. Proc. Biol. Sci. 289, 20221090.
Lavering, I.H., 1993. Quaternary and modern environments of the Van Diemen Rise, Timor Sea, and potential effects of additional petroleum exploration activity. BMR J. Aust. Geol. Geophys. 13, 281–292.
Leatherwood, S., Reeves, R.R., Perrin, W.F., Evans, W.E., 1982. Whales, dolphins, and porpoises of the eastern North Pacific and adjacent Arctic waters: a guide to their identification. NOAA Technical Report NMFS Circular, Rockville.
Macleod, C.D., Reidenberg, J.S., Weller, M., Santos, M.B., Herman, J., Goold, J., Pierce, G.J., 2007. Breaking symmetry: the marine environment, prey size, and the evolution of asymmetry in cetacean skulls. Anat. Rec. 290, 539–545.
Madsen, P., Kerr, I., Payne, R., 2004. Echolocation clicks of two free-ranging, oceanic delphinids with different food preferences: false killer whales. *Pseudorca crassidens* and Risso's dolphins *Grampus griseus*. J. Exp. Biol. 207, 1811–1823.
Madsen, P.T., Wahlberg, M., Møhl, B., 2002. Male sperm whale (*Physeter macrocephalus*) acoustics in a high-latitude habitat: implications for echolocation and communication. Behav. Ecol. Sociobiol. 53, 31–41.
Madsen, P.T., Carder, D.A., Beedholm, K., Ridgway, S.H., 2005. Porpoise clicks from a sperm whale nose - convergent evolution of 130 kHz pulses in toothed whale sonars? Bioacoustics 15, 195–206.
Madsen, P.T., Wisniewska, D., Beedholm, K., 2010. Single source sound production and dynamic beam formation in echolocating harbour porpoises (*Phocoena phocoena*.). J. Exp. Biol. 213, 3105–3110.
Madsen, P.T., Lammers, M., Wisniewska, D., Beedholm, K., 2013. Nasal sound production in echolocating delphinids (*Tursiops truncatus* and *Pseudorca crassidens*) is dynamic, but unilateral: clicking on the right side and whistling on the left side. J. Exp. Biol. 216, 4091–4102.
Madsen, P.T., Siebert, U., Elemans, C.P.H., 2023. Toothed whales use distinct vocal registers for echolocation and communication. Science 379, 928–933.
Malinka, C.E., Tønnesen, P., Dunn, C.A., Claridge, D.E., Gridley, T., Elwen, S.H., Madsen, P.T., 2021. Echolocation click parameters and biosonar behaviour of the dwarf sperm whale (*Kogia sima*). J. Exp. Biol. 224, jeb240689.
Marx, F.G., Lambert, O., Uhen, M.D., 2016. Cetacean Paleobiology. Wiley, Oxford.
McGowen, M.R., Tsagkogeorga, G., Álvarez-Carretero, S., Reis, M., Struebig, M., Deaville, R., Jepson, P.D., Jarman, S., Polanowski, A., Morin, P.A., Rossiter, S.J., 2020. Phylogenomic resolution of the cetacean tree of life using target sequence capture. Syst. Biol. 69, 479–501.
Mckenna, M.F., Cranford, T.W., Berta, A., Pyenson, N.D., 2012. Morphology of the odontocete melon and its implications for acoustic function. Mar. Mamm. Sci. 28, 690–713.
Mead, J.G., 1975. Anatomy of the external nasal passages and facial complex in the Delphinidae (Mammalia: Cetacea). Smithsonian Contributions to Zoology. Smithsonian Institution Press, Washington D.C.
Mead, J.G., Fordyce, R.E., 2009. The therian skull: a lexicon with emphasis on the odontocetes. Smithsonian Contributions to Zoology. Smithsonian Institution Scholarly Press, Washington D.C.
Melcón, M.L., Failla, M., Iñíguez, M.A., 2012. Echolocation behavior of franciscana dolphins (*Pontoporia blainvillei*) in the wild. J. Acoust. Soc. Am. 131, 448–453.
Milinkovitch, M.C., Meyer, A., Powell, J.R., 1994. Phylogeny of all major groups of cetaceans based on DNA sequences from three mitochondrial genes. Mol. Biol. Evol. 11, 939–948.
Miller, F.P., Vandome, A.F., McBrewster, J., 2009. Brahmaputra River. Alphascript Publishing,.
Miller, P.J.O., Kvadsheim, P.H., Lam, F.P.A., Tyack, P.L., Curé, C., DeRuiter, S.L., Kleivane, L., Sivle, L.D., van Ijsselmuide, S.P., Visser, F., Wensveen, P.J., von Benda-Beckmann, A.M., Martín López, L.M., Narazaki, T., Hooker, S.K., 2015. First indications that northern bottlenose whales are sensitive to behavioural disturbance from anthropogenic noise. R. Soc. Open Sci. 2, 140484.
Minamikawa, S., Iwasaki, T., Tanaka, Y., Ryono, A., Noji, S., Sato, H., Kato, H., 2003. Diurnal pattern of diving behavior in striped dolphins, *Stenella coeruleoalba*. I Int. Symp. Bio-Logging Sci. 23–24.
Minamikawa, S., Iwasaki, T., Kishiro, T., 2007. Diving behaviour of a Baird's beaked whale, *Berardius bairdii*, in the slope water region of the western North Pacific: first dive records using a data logger. Fish. Oceanogr. 16, 573–577.
Møhl, B., Wahlberg, M., Madsen, P.T., Heerfordt, A., Lund, A., 2003. The monopulsed nature of sperm whale clicks. J. Acoust. Soc. Am. 114, 1143–1154.

Monteiro-Filho, E.L.D., Monteiro, L.R., Reis, S.F., 2002. Skull shape and size divergence in dolphins of the genus *Sotalia*: a tridimensional morphometric analysis. J. Mamm. 83, 125–134.
Morisaka, T., Karczmarski, L., Akamatsu, T., Sakai, M., Dawson, S., Thornton, M., 2011. Echolocation signals of Heaviside's dolphins (*Cephalorhynchus heavisidii*.). J. Acoust. Soc. Am. 129, 449–457.
Mullin, K.D., Higgins, L.V., Jefferson, T.A., Hansen, L.J., 1994. Sightings of the Clymene dolphin (*Stenella clymene*) in the Gulf of Mexico. Mar. Mamm. Sci. 10, 464–470.
Murakami, M., Shimada, C., Hikida, Y., Hirano, H., 2014. Asymmetrical basal delphinoid skull from the upper lower Miocene Yamato formation of Hokkaido, Northern Japan: implications on evolution of cranial asymmetry and symmetry in Odontoceti. Paleontol. Res. 18, 134–149.
Ness, A.R., 1967. A measure of asymmetry of skulls of odontocete whales. J. Zool. 153, 209–221.
Neville, A.C., 1976. Animal Asymmetry. Edward Arnold, London.
Nielsen, N.H., Teilmann, J., Sveegaard, S., Hansen, R.G., Sinding, M.H.S., Dietz, R., Heide-Jørgensen, M.P., 2018. Oceanic movements, site fidelity and deep diving in harbour porpoises from Greenland show limited similarities to animals from the North Sea. Mar. Ecol. Prog. Ser. 597, 259–272.
NOAA - National Oceanic and Atmospheric Administration Fisheries, 2022a. *Mesoplodon bidens*. Available at: ⟨https://www.fisheries.noaa.gov/species/sowerbys-beaked-whale⟩.
NOAA - National Oceanic and Atmospheric Administration Fisheries, 2022b. *Mesoplodon stejnegeri.* Available at: ⟨https://www.fisheries.noaa.gov/species/stejnegers-beaked-whale⟩.
Pagel, M.D., 1999. Inferring the historical patterns of biological evolution. Nature.
Palmer, A.R., 2009. Animal asymmetry. Curr. Biol. 19, 473–477.
Paradis, E., Blomberg, S., Bolker, B., Brown, J., Claramunt, S., Claude, J., Cuong, H.S., Desper, R., Didier, G., Durand, B., Dutheil, J., Ewing, R.J., Gascuel, O., Guillerme, T., Heibl, C., Ives, A., Jones, B., Krah, F., Lawson, D., Lefort, V., Legendre, P., Lemon, J., Louvel, G., Marcon, E., McCloskey, R., Nylander, J., Opgen-Rhein, R., Popescu, A.A., Royer-Carenzi, M., Schliep, K., Strimmer, K., Vienne, D., 2020. Ape: Anal. phylogenetics Evol. R. Package Version 5. 4 (Available at). ⟨https://CRAN.R-project.org/package=ape⟩.
Parra, G.J., 2006. Resource partitioning in sympatric delphinids: space use and habitat preferences of Australian snubfin and Indo-Pacific humpback dolphins. J. Anim. Ecol. 75, 862–874.
Parra, G.J., Jefferson, T.A., 2018. Humpback dolphins *Sousa teuszii*, *S. plumbea*, *S. chinensis* and *S. sahulensis*. In: Würsig, B., Thewissen, J.G.M., Kovacs, K. (Eds.), Encyclopedia of Marine Mammals, third ed. Academic Press, London, pp. 483–489.
Pedersen, M.B., Tønnesen, P., Malinka, C.E., Ladegaard, M., Johnson, M., Aguilar Soto, N., Madsen, P.T., 2021. Echolocation click parameters of short-finned pilot whales (*Globicephala macrorhynchus*) in the wild. J. Acoust. Soc. Am. 149, 1923–1931.
Pinheiro, J., Bates, D., DebRoy, S., Sarkar, D., 2021. Nlme: linear and nonlinear mixed effects models. R Package version 3.1–153 Available at: https://CRAN.R-project.org/package=nlme.
Perrin, W.F., 2009. Spinner dolphin *Stenella longirostris*. In: Perrin, W.P., Würsig, B., Thewissen, J.G.M.(Eds.) (Eds.), Encyclopedia of Marine Mammals, second ed. Academic Press, San Diego, California, pp. 1100–1103.
Plön, S., 2004. The status and natural history of pygmy (*Kogia breviceps*) and dwarf (*K. sima*) sperm whales off Southern Africa. PhD thesis. Rhodes University,.
Pulis, E.E., Wells, R.S., Schorr, G.S., Douglas, D.C., Samuelson, M.M., Solangi, M., 2018. Movements and dive patterns of pygmy killer whales (*Feresa attenuata*) released in the Gulf of Mexico following rehabilitation. Aquat. Mamm. 44, 555–567.
R Core Team, 2022. R: A language and environment for statistical computing. R Foundation for Statistical Computing,, Viena (Available at). ⟨https://cran.r-project.org/⟩.
Rasmussen, M.H., Koblitz, J.C., Laidre, K.L., 2015. Buzzes and high-frequency clicks recorded from narwhals (*Monodon monoceros*) at their wintering ground. Aquat. Mamm. 41, 256–264.
Reisinger, R.R., Keith, M., Andrews, R.D., De Bruyn, P.J.N., 2015. Movement and diving of killer whales (*Orcinus orca*) at a Southern Ocean archipelago. J. Exp. Mar. Biol. Ecol. 473, 90–102.
Reyes, J.C., 2009. Burmeister's Porpoise *Phocoena spinipinnis*. In: Perrin, W.P., Würsig, B., Thewissen, J.G.M. (Eds.), Encyclopedia of Marine Mammals, second ed. Academic Press, San Diego, California, pp. 163–167.
Reyes, M.V.R., Reyes, V., Marino, A., Dellabianca, N.A., Hevia, M., Torres, M., Rey, A.R., Melcón, M.L., 2018. Clicks of wild Burmeister's porpoises (*Phocoena spinipinnis*) in Tierra del Fuego, Argentina. Mar. Mamm. Sci. 34, 1070–1081.
Richard, P.R., Martin, A.R., Orr, J.R., 1998. Study of later summer and fall movements and dive behavior of Beaufort Sea belugas, using satellite telemetry: 1997. MMS OCS Study 98–0016, Anchorage.
Rohlf, F.J., 2015. The tps series of software. Hystrix 26, 9–12.
Rohlf, F.J., Slice, D., 1990. Extensions of the Procrustes method for the optimal superimposition of landmarks. Syst. Zool. 39, 40–59.
Sabin, R., Burton, K., Cooper, N., Goswami, A., 2018. Dataset: 3D cetacean scanning (Available at). Nat. Hist. Mus. Data Portal (Data. nhm. ac. uk). https://doi.org/10.5519/0020467.
Schenkkan, E.J., 1973. On the comparative anatomy and function of the nasal tract in odontocetes (Mammalia, Cetacea). Bijdr. Dierkd. 43, 127–159.
Schorr, G.S., Falcone, E.A., Moretti, D.J., Andrews, R.D., 2014. First long-term behavioral records from Cuvier's beaked whales (*Ziphius cavirostris*) reveal record-breaking dives. PLoS One 9, e92633.
Schotten, M., Au, W.W.L., Lammers, M.O., Aubauer, R., 2004. Echolocation recordings and localization of wild spinner dolphins (*Stenella longirostris*) and pantropical spotted dolphins (*S. attenuata*) using a four-hydrophone array. In: Thomas, J.A., Moss, C.F., Vater, M. (Eds.), Echolocation in Bats and Dolphins. University of Chicago Press, Chicago, pp. 393–400.
Shaff, J.F., Baird, R.W., 2021. Diel and lunar variation in diving behavior of rough-toothed dolphins (*Steno bredanensis*) off Kaua'i, Hawai'i. Mar. Mamm. Sci. 37, 1261–1276.
Sheets, H.D., 2007. VecCompare6. Integrated Morphometrics Package (IMP) 6. Available at: ⟨https://www.animal-behaviour.de/imp/⟩.
Silber, G.K., 1990. Occurrence and distribution of the vaquita (*Phocoena sinus*) in the northern Gulf of California. Fish. Bull. (U. S.) 88, 339–346.
Sioli, H., 1984. The Amazon: limnology and landscape ecology of a mighty tropical river and its basin. Dr W. Junk Publishers, Dordrecht.
Stacey, B.P., Arnold, P.W., 1999. Orcaella brevirostris. Mamm. Species 616, 1–8.
Stimpert, A.K., DeRuiter, S.L., Southall, B.L., Moretti, D.J., Falcone, E.A., Goldbogen, J. A., Friedlaender, A., Schorr, G.S., Calambokidis, J., 2014. Acoustic and foraging behavior of a Baird's beaked whale, *Berardius bairdii*, exposed to simulated sonar. Sci. Rep. 4, 7031.
Sydney, N.V., 2010. Ontogenia e assimetria craniana, *Sotalia guianensis* (Cetacea: Delphinidae). Master thesis. Universidade de São Paulo.
Thewissen, J.G.M., 2009. Sendory biology: overwiew. In: Perrin, W.P., Würsig, B., Thewissen, J.G.M. (Eds.), Encyclopedia of Marine Mammals, 2ed.,. Academic Press, San Diego, California, pp. 1003–1005.
Thewissen, J.G.M., Williams, E.M., Roe, L.J., Hussain, S.T., 2001. Skeletons of terrestrial cetaceans and the relationship of whales to artiodactyls. Nature 413, 277–281.
Tyack, P.L., Johnson, M., Aguilar Soto, N., Sturlese, A., Madsen, P.T., 2006. Extreme diving of beaked whales. J. Exp. Biol. 209, 4238–4253.
Velez-Juarbe, J., Wood, A.R., De Gracia, C., Hendy, A.J.W., 2015. Evolutionary patterns among living and fossil kogiid sperm whales: evidence from the Neogene of Central America. PLoS One 10, e0123909.
Vicari, D., McGowen, M.R., Lambert, O., Brown, R.P., Bianucci, G., Sabin, R., Meloro, C., 2023. Ecomorphology of toothed whales (Cetacea, Odontoceti) as revealed by 3D skull geometry (Available at). J. Mamm. Evol.. https://doi.org/10.1007/s10914-022-09642-4.
Visser, F., Keller, O.A., Oudejans, M.G., Nowacek, D.P., Kok, A.C.M., Huisman, J., Sterck, E.H.M., 2021. Risso's dolphins perform spin dives to target deep-dwelling prey. R. Soc. Open Sci. 8, 202320.
Waddell, V.G., Milinkovitch, M.C., Bérubé, M., Stanhope, M.J., 2000. Molecular phylogenetic examination of the Delphinoidea trichotomy: congruent evidence from three nuclear loci indicates that porpoises (Phocoenidae) share a more recent common ancestry with white whales (Monodontidae) than they do with true dolphins (Delphinidae). Mol. Phylogenetics Evol. 15, 314–318.
Wahlberg, M., Beedholm, K., Heerfordt, A., Møhl, B., 2011a. Characteristics of biosonar signals from the northern bottlenose whale, *Hyperoodon ampullatus*. J. Acoust. Soc. Am. 130, 3077–3084.
Wahlberg, M., Jensen, F.H., Aguilar Soto, N., Beedholm, K., Bejder, L., Oliveira, C., Rasmussen, M., Simon, M., Villadsgaard, L., Madsen, P.T., 2011b. Source parameters of echolocation clicks from wild bottlenose dolphins (*Tursiops aduncus* and *Tursiops truncatus*.). J. Acoust. Soc. Am. 130, 2263–2274.
Wang, J.Y., Yang, S.H., 2009. Indo-Pacific bottlenose dolphin *Tursiops aduncus*. In: Perrin, W.P., Würsig, B., Thewissen, J.G.M. (Eds.), Encyclopedia of Marine Mammals, 2ed..,. Academic Press, San Diego, California, pp. 602–608.
West, K.L., Walker, W.A., Baird, R.W., Webster, D.L., Schorr, G.S., 2018. Stomach contents and diel diving behavior of melon-headed whales (*Peponocephala electra*) in Hawaiian waters. Mar. Mamm. Sci. 34, 1082–1096.
Winn, H.E., 1982. A characterization of marine mammals and turtles in the mid- and North Atlantic areas of the United States upper continental shelf, final report. Bureau of Land Management, Washington D.C.
Yamamoto, Y., Akamatsu, T., da Silva, V.M.F., Yoshida, Y., Kohshima, S., 2015. Acoustic characteristics of biosonar sounds of free-ranging botos (*Inia geoffrensis*) and tucuxis (*Sotalia fluviatilis*) in the Negro River, Amazon, Brazil. J. Acoust. Soc. Am. 138, 687–693.
Yurick, D.B., Gaskin, D.E., 1988. Asymmetry in the skull of the harbour porpoise *Phocoena phocoena* (L.) and its relationship to sound production and echolocation. Can. J. Zool. 66, 399–402.
Zelditch, M.L., Swiderski, D.L., Sheets, H.D., 2012. Geometric morphometrics for biologists: a primer, second ed. Elsevier Academic Press, San Diego.
Zhou, K., 2009. Baiji: *Lipotes vexillifer*. In: Perrin, W.P., Würsig, B., Thewissen, J.G.M. (Eds.) (Eds.), Encyclopedia of Marine Mammals, second ed. Academic Press, San Diego, California, pp. 71–76.
Zimmer, W.M.X., Madsen, P.T., Teloni, V., Johnson, M.P., Tyack, P.L., 2005a. Off-axis effects on the multipulse structure of sperm whale usual clicks with implications for sound production. J. Acoust. Soc. Am. 118, 3337–3345.
Zimmer, W.M.X., Johnson, M.P., Madsen, P.T., Tyack, P.L., 2005b. Echolocation clicks of free-ranging Cuvier's beaked whales (*Ziphius cavirostris)*. J. Acoust. Soc. Am. 117, 3919–3927.